

LINEAR, SECOND ORDER AND UNCONDITIONALLY ENERGY STABLE SCHEMES FOR A PHASE-FIELD MOVING CONTACT LINE MODEL

XIAOFENG YANG [†] AND HAIJUN YU ^{‡,*}

ABSTRACT. In this paper, we consider the numerical approximations for solving a hydrodynamics coupled phase field model consisting of incompressible Navier-Stokes equations with generalized Navier boundary conditions, and the Cahn-Hilliard equation with dynamic moving contact line boundary conditions. The main challenging issue for solving this model numerically is the time marching problem, i.e., how to develop suitable higher order temporal schemes while preserving the unconditional energy stability at the discrete level. We solve this issue by developing two linear, second-order schemes based on the “Invariant Energy Quadraticization” method for the nonlinear terms in the bulk and on the boundary, the projection method for the Navier-Stokes equations, and a subtle implicit-explicit treatment for the stress and convective terms. Rigorous proofs of the well-posedness of the linear system and the unconditional energy stabilities are provided. A spectral-Galerkin spatial discretization is implemented and various numerical results are presented to verify the second order accuracy and the efficiency of the proposed schemes.

1. INTRODUCTION

In this paper, we consider numerical approximations for a hydrodynamics coupled phase field model [42–44] with moving contact line (MCL) boundary conditions. The phase field method is a popular approach that is widely used to simulate the interfacial dynamics of multiple material components due to its versatility in modeling as well as numerical simulations (cf. [2, 16, 24, 27, 28, 31, 32, 34, 37, 39, 55, 58, 59, 63, 64]). The fluid-fluid interface in this method is considered as a continuous, but steep change of some physical properties of two fluid components, e.g., density or viscosity, etc. An order parameter (or called phase field variable) is introduced to label the two fluid components, thus the interface is then represented by a thin but smooth transition layer that can remove the singularities in practice. The standard phase field model for multiple incompressible fluid mixture is a nonlinear system that couples the Cahn-Hilliard equation and the Navier-Stokes equations via convective and stress terms, see also [15, 20, 32, 35] for two phase flow case and [2–4, 28, 76] for three or more phase flow case.

Once the fluid-fluid interface touches a solid wall, a MCL problem is induced. This phenomenon exists in many physical and engineering processes such as wetting, coating, or painting, etc. In this situation, the no-slip boundary condition for the Navier-Stokes equations is no longer applicable (cf. [9, 10, 40]). Simulations in [29, 30, 61] using molecular dynamics simulations showed that nearly complete slip happens near the MCL. In the context of phase field method, a set of accurate boundary conditions for the MCL problem was derived by Wang and Qian et. al. in [42–44], resulting in a standard two phase model supplemented with a generalized Navier boundary condition (GNBC)

Key words and phrases. Phase field, Cahn-Hilliard, Moving contact line, Unconditional energy stability, Second order scheme, Invariant energy quadraticization.

[†]Department of Mathematics, University of South Carolina, Columbia, SC, USA 29208. Email: xfyang@math.sc.edu

^{*}Corresponding author, NCMIS & LSEC, Institute of Computational Mathematics, Academy of Mathematics and Systems Science, Beijing 100190, China. Email: hyu@lsec.cc.ac.cn.

[‡]School of Mathematical Sciences, University of Chinese Academy of Sciences, Beijing 100049, China.

and a dynamic contact line condition (DCLC), where the nonlinear couplings also show up in the boundary conditions.

Numerically, although the phase field variable is continuous and smooth, the model is still very stiff since a small dimensionless parameter related to the thickness of the interface layer, is involved, for which certain numerical methods like fully implicit or explicit type methods (cf. [14, 51]) for nonlinear terms, are numerically unstable. Hence a challenging issue for solving the model is to develop numerically stable methods, namely, to establish efficient numerical schemes that can verify the so-called energy stable property at the discrete level, irrespective of the coarseness of the discretization. Such a kind of algorithms is usually called unconditionally energy stable or thermodynamically consistent. The scheme with this property is specially preferred since it is not only critical for the numerical scheme to use larger time steps to capture the correct long time dynamics that can reduce the time cost in computing, but also provides sufficient flexibility for dealing with the stiffness issue. Nonetheless, we need mention a basic fact that a larger time step will definitely induce larger numerical errors. In other words, schemes with unconditional energy stability can allow arbitrarily large time step only for the sake of the stability concern. To measure whether a scheme is reliable or not, the controllable accuracy is another important factor except the stability. Therefore, if one attempts to use a time step as large as possible while maintaining the desirable accuracy, the only possible choice is to develop more accurate schemes, e.g., second order energy stable schemes, that is the main focus of this paper.

It is remarkable that, unlike the enormous numerical scheme developments on the standard phase field model for two phase fluid flows system with easy boundary conditions (without MCLs), e.g., see [13, 24, 28, 31, 32, 37, 58, 60, 77, 79], almost all developed time marching schemes for solving the model with MCLs are first order, e.g., see [1, 7, 8, 16, 17, 23, 36, 45, 56, 74]. More precisely, to the best of the authors' knowledge, no schemes can be claimed to possess the following three properties, namely, *easy-to-implement*, *unconditionally energy stable* and *second order accuracy*. Here the term "easy-to-implement" is referred to "linear" and/or "decoupled" in comparison with its counter parts: "nonlinear" and/or "coupled". This is because two additional numerical difficulties, the discretization of the GNBC and DCLC conditions on the boundary, emerge besides the regular stiffness issue induced by the nonlinear double well potential in the Cahn-Hilliard equation. At the very least, even for the Cahn-Hilliard equation, the algorithm design is still challenging. It can be seen clearly from a fact that a severe stability constraint of the time step on the interfacial width occurs if the nonlinear term is discretized in some normal ways like fully implicit or explicit type approaches [14, 51, 65], which in turn can cause high computational cost in practice. To overcome the stiffness issue, many efforts had been implemented to remove the time step constraint, including, e.g., the nonlinear convex splitting approach [12, 48, 57, 64], and the linear stabilization approach [6, 33, 34, 41, 47, 49–54, 56, 67, 68, 76–79]. About the pros and cons of these two methods, we give some detailed discussions in Section 3.

Therefore, the aim of this paper is to develop some more efficient and accurate schemes for solving the phase-field MCL model in [42–44]. We shall construct second order time stepping schemes which satisfy a discrete energy law by combining several successful approaches including the *Invariant Energy Quadratization* (IEQ) method (cf. [21, 66, 69, 70, 72]) for nonlinear terms that appear in the bulk as well as the boundary for the phase field equation, the *projection method* for the Navier-Stokes equations to decouple the velocity and pressure, and a subtle *implicit-explicit* treatment for the stress and convective terms. At each time step, one can solve a linear elliptic system for the phase variable and the velocity field, and a Poisson equation for the pressure. We shall give rigorous proofs of the well-posedness of the linear system together with the energy stabilities, and implement

the schemes using the spectral-Galerkin method in space to verify the second order accuracy in time and the efficiency.

The rest of the paper is organized as follows. In Section 2, we briefly describe the phase field model with MCL boundary conditions and derive its associated PDE energy dissipation law. In Section 3, we present the numerical schemes, and prove the well-posedness of the semi-discretized linear system and their discrete energy dissipation law rigorously. In Section 4, we describe the spatial discretization method using the spectral-Galerkin (Fourier-Legendre basis) approach. In section 5, we present various numerical examples to illustrate the accuracy and efficiency of the proposed schemes. Some concluding remarks are given in Section 6.

2. THE PDE SYSTEM AND ITS ENERGY LAW

We now describe the phase-field model for a mixture of two immiscible, incompressible fluids in a confined domain $\Omega \subset \mathbb{R}^d$ ($d = 2, 3$) with matched density and viscosity. We introduce a phase field variable (macroscopic labeling function) $\phi(\mathbf{x}, t)$ such that

$$(2.1) \quad \phi(\mathbf{x}, t) = \begin{cases} 1, & \text{fluid I,} \\ -1, & \text{fluid II,} \end{cases}$$

with a thin, smooth transition region of width $O(\epsilon)$, and consider the following Ginzburg-Landau type of Helmholtz free energy functional:

$$(2.2) \quad E_{mix} = \lambda \int_{\Omega} \left(\frac{\epsilon}{2} |\nabla \phi|^2 + F(\phi) \right) d\mathbf{x},$$

where λ denotes rescaled characteristic strength of phase mixing energy. The first gradient term in E_{mix} contributes to the hydro-philic type (tendency of mixing) of interactions between the materials and the second part, the double well bulk energy $F(\phi) = \frac{1}{4\epsilon}(\phi^2 - 1)^2$, represents the hydro-phobic type (tendency of separation) of interactions. As the consequence of the competition between the two types of interactions, the equilibrium configuration will include a diffusive interface with a thickness proportional to the parameter ϵ .

The total energy of the hydrodynamic system is a sum of the kinetic energy E_k together with the mixing energy E_{mix} :

$$(2.3) \quad E = E_k + E_{mix} = \int_{\Omega} \left(\frac{1}{2} |\mathbf{u}|^2 + \lambda \left(\frac{\epsilon}{2} |\nabla \phi|^2 + F(\phi) \right) \right) d\mathbf{x}.$$

Here \mathbf{u} is the fluid velocity field, and we assume the fluid density is 1.

The evolution of the phase function is governed by the Cahn-Hilliard equation in the conserved form as follows,

$$(2.4) \quad \phi_t + \nabla \cdot (\mathbf{u}\phi) = M\Delta\mu,$$

$$(2.5) \quad \mu = \lambda(-\epsilon\Delta\phi + f(\phi)),$$

where μ is the chemical potential, M is a mobility parameter related to the relaxation time scale, and $f(\phi) = F'(\phi) = \frac{1}{\epsilon}\phi(\phi^2 - 1)$.

The momentum equation (macroscopic force balance) for the hydrodynamics takes the usual form of the Navier-Stokes equation as follows (cf. [2, 3, 16, 28, 31, 32, 34, 55]),

$$(2.6) \quad \mathbf{u}_t + (\mathbf{u} \cdot \nabla)\mathbf{u} - \nu\Delta\mathbf{u} + \nabla p + \phi\nabla\mu = 0,$$

$$(2.7) \quad \nabla \cdot \mathbf{u} = 0,$$

where p is the pressure, ν is the kinetic viscosity of the mixture. Note that the stress term is written as $\phi \nabla \mu$ instead of the $-\mu \nabla \phi$ in most other references. This is due to $\phi \nabla \mu = \nabla(\phi \mu) - \mu \nabla \phi$, and the $\nabla(\phi \mu)$ can be absorbed into the pressure.

For the boundary conditions, if the fluid-fluid interface never touches the wall (domain boundary Γ), we can assume the easy no-slip boundary conditions

$$(2.8) \quad \mathbf{u}|_{\Gamma} = \mathbf{u}_w, \quad \partial_{\mathbf{n}} \phi|_{\Gamma} = 0, \quad \partial_{\mathbf{n}} \mu|_{\Gamma} = 0.$$

where \mathbf{n} is the outward normal on the domain boundary Γ , \mathbf{u}_w is the boundary wall velocity.

If the fluid-fluid interface touches the wall, the MCL problem appears. On the boundary Γ , we have the GNBC for the velocity as follows,

$$(2.9) \quad \mathbf{u} \cdot \mathbf{n} = 0,$$

$$(2.10) \quad \nu \partial_{\mathbf{n}} \mathbf{u}_{\tau} = -\nu \ell(\phi)(\mathbf{u}_{\tau} - \mathbf{u}_w) - \frac{\lambda}{\gamma} \dot{\phi} \nabla_{\tau} \phi,$$

and together with the DCLC for the phase field variable on the boundary Γ (cf. [16,17,42,44,56,74]),

$$(2.11) \quad \partial_{\mathbf{n}} \mu = 0,$$

$$(2.12) \quad \epsilon \partial_{\mathbf{n}} \phi = -\frac{1}{\gamma} \dot{\phi} - g(\phi),$$

where $\dot{\phi} = \phi_t + \mathbf{u}_{\tau} \cdot \nabla_{\tau} \phi$, $\ell(\phi) \geq 0$ is a given coefficient function that is the ratio of domain length to the slip length, γ is a boundary relaxation coefficient, \mathbf{u}_w is the wall velocity, \mathbf{u}_{τ} is the tangential velocity along the boundary tangential direction τ , $\nabla_{\tau} = \nabla - (\mathbf{n} \cdot \nabla) \mathbf{n}$ is the gradient along τ , $g(\phi) = G'(\phi)$ and $G(\phi)$ is the interfacial energy that is defined as

$$(2.13) \quad G(\phi) = -\frac{\sqrt{2}}{3} \cos \theta_s \sin \left(\frac{\pi}{2} \phi \right),$$

where θ_s is the static contact angle. From (2.9), we have $\mathbf{u} = \mathbf{u}_{\tau}$ on boundary Γ .

About the validity of the Navier-Stokes-Cahn-Hilliard (NSCH) phase field model (2.4)-(2.5)-(2.6)-(2.7) with boundary conditions of GNBC (2.9)-(2.10) and DCLC (2.11)-(2.12), we refer to a series of modeling and analysis work of Qian and Wang et. al. in [42-44].

We now derive the PDE energy dissipation law for the above model. Here and after, for any function $f, g \in L^2(\Omega)$, we use $(f, g) = \int_{\Omega} f(\mathbf{x})g(\mathbf{x})d\mathbf{x}$ to denote the L^2 inner product between functions $f(\mathbf{x})$ and $g(\mathbf{x})$, $(f, g)_{\Gamma}$ to denote $\int_{\Gamma} f(s)g(s)ds$, and $\|f\|^2 = (f, f)$ and $\|f\|_{\Gamma}^2 = (f, f)_{\Gamma}$.

Lemma 2.1. *The NSCH system with GNBC and DCLC ((2.4)-(2.7) with (2.9)-(2.12)) is a dissipative system satisfying the following energy dissipation law*

$$(2.14) \quad \frac{d}{dt} E_{tot} = -\nu \|\nabla \mathbf{u}\|^2 - M \|\nabla \mu\|^2 - \frac{\lambda}{\gamma} \|\dot{\phi}\|_{\Gamma}^2 - \nu \|\sqrt{\ell(\phi)} \mathbf{u}_s\|_{\Gamma}^2 - \nu (\ell(\phi) \mathbf{u}_s, \mathbf{u}_w)_{\Gamma},$$

where $\mathbf{u}_s = \mathbf{u} - \mathbf{u}_w$ is the velocity slip on boundary Γ and

$$(2.15) \quad E_{tot}(\mathbf{u}, \phi) = \int_{\Omega} \left(\frac{1}{2} |\mathbf{u}|^2 + \lambda \left(\frac{\epsilon}{2} |\nabla \phi|^2 + F(\phi) \right) \right) d\mathbf{x} + \lambda \int_{\Gamma} G(\phi(s)) ds.$$

Proof. By taking the L^2 inner product of equation (2.4) with μ , and using boundary conditions (2.9) and (2.11), we get

$$(2.16) \quad (\phi_t, \mu) - (\mathbf{u} \phi, \nabla \mu) = -M \|\nabla \mu\|^2.$$

By taking the L^2 inner product of equation (2.5) with $-\phi_t$, we have

$$(2.17) \quad -(\mu, \phi_t) = \lambda \epsilon (\partial_{\mathbf{n}} \phi, \phi_t)_{\Gamma} - \frac{\lambda \epsilon}{2} \frac{d}{dt} \|\nabla \phi\|^2 - \lambda \frac{d}{dt} (F(\phi), 1).$$

By taking the L^2 inner product of equation (2.6) with \mathbf{u} and using the divergence free condition (2.7), we get

$$(2.18) \quad \frac{d}{dt} \frac{\|\mathbf{u}\|^2}{2} = -\nu \|\nabla \mathbf{u}\|^2 + \nu (\partial_{\mathbf{n}} \mathbf{u}_\tau, \mathbf{u}_\tau)_\Gamma - (\phi \nabla \mu, \mathbf{u}).$$

By taking the summation of (2.16)-(2.18), we obtain

$$(2.19) \quad \frac{d}{dt} \left(\frac{1}{2} \|\mathbf{u}\|^2 + \lambda \left(\frac{\epsilon}{2} \|\nabla \phi\|^2 + (F(\phi), 1) \right) \right) = -\nu \|\nabla \mathbf{u}\|^2 - M \|\nabla \mu\|^2 + (\nu \partial_{\mathbf{n}} \mathbf{u}, \mathbf{u})_\Gamma + \lambda (\epsilon \partial_{\mathbf{n}} \phi, \phi_t)_\Gamma.$$

Then, using boundary condition (2.10) and (2.12), we derive

$$(2.20) \quad \begin{aligned} (\nu \partial_{\mathbf{n}} \mathbf{u}, \mathbf{u})_\Gamma &= (\nu \partial_{\mathbf{n}} \mathbf{u}_\tau, \mathbf{u}_\tau)_\Gamma \\ &= \left(-\nu \ell(\phi) (\mathbf{u}_\tau - \mathbf{u}_w) - \frac{\lambda}{\gamma} \dot{\phi} \nabla_\tau \phi, \mathbf{u}_\tau \right)_\Gamma \\ &= -\nu (\ell(\phi) \mathbf{u}_s, \mathbf{u}_s + \mathbf{u}_w)_\Gamma - \frac{\lambda}{\gamma} (\dot{\phi} \nabla_\tau \phi, \mathbf{u}_\tau)_\Gamma, \end{aligned}$$

and

$$(2.21) \quad \begin{aligned} \lambda (\epsilon \partial_{\mathbf{n}} \phi, \phi_t)_\Gamma &= \lambda \left(-\frac{1}{\gamma} \dot{\phi} - g(\phi), \phi_t \right)_\Gamma \\ &= -\frac{\lambda}{\gamma} (\dot{\phi}, \dot{\phi} - \mathbf{u}_\tau \cdot \nabla_\tau \phi)_\Gamma - \lambda (g(\phi), \phi_t)_\Gamma \\ &= -\frac{\lambda}{\gamma} \|\dot{\phi}\|_\Gamma^2 + \frac{\lambda}{\gamma} (\dot{\phi}, \mathbf{u}_\tau \cdot \nabla_\tau \phi)_\Gamma - \lambda \frac{d}{dt} (G(\phi), 1)_\Gamma. \end{aligned}$$

Summing up (2.19), (2.20), and (2.21), we get the desired energy law (2.14). \square

Remark 2.1. The NSCH system with DCLC and GNBC reduces to a system with static contact line conditions and Navier boundary conditions when $\gamma \rightarrow +\infty$ in (2.12), i.e.,

$$(2.22) \quad \begin{aligned} \epsilon \partial_{\mathbf{n}} \phi + g(\phi) &= 0, \\ \partial_{\mathbf{n}} \mathbf{u}_\tau &= -\ell(\phi) (\mathbf{u}_\tau - \mathbf{u}_w). \end{aligned}$$

If we further set $\ell(\phi) \rightarrow +\infty$ and $G(\phi) = 0$, then the system reduces to the standard Cahn-Hilliard phase field without contact lines and fluid equation with no-slip boundary condition. Therefore, we only need to develop efficient numerical methods for the NSCH system with DCLC and GNBC, the other situations can be covered by tuning corresponding parameters.

Remark 2.2. The boundary energy density (2.13) is a smooth interpolation between the boundary energy density in $\phi = +1$ and $\phi = -1$ region. It is commonly used in modeling and simulations of MCL problems, e.g., [1, 16, 17, 23, 23, 36, 42, 44, 45, 56]. Since $G(\phi)$ defined in (2.13) has a lower bound, the system energy defined in (2.15) has a lower bound. Another type of boundary energy density is also widely used in literature (cf. [7, 26, 75]),

$$(2.23) \quad G(\phi) = c_0 + c_1 (\phi^3 - 3\phi) \cos \theta_s,$$

where c_0 is a constant which is not relevant to the PDEs, $c_1 = \frac{\sqrt{2}}{6}$ such that the equilibrium solution induced by the boundary energy is consistent to the one induced by bulk energy. However, such a boundary energy has no lower bound, thus the stability of the solution for the corresponding PDE system may not be ensured. A possible solution is to modify this energy outside of domain $[-1, 1]$

since those parts are not “physically” relevant. For instance, such modification can be given as

$$(2.24) \quad G(\phi) = \begin{cases} c_0 + c_1(\phi^3 - 3\phi) \cos \theta_s, & |\phi| \leq 1, \\ c_0 + 2c_1 \cos \theta_s, & \phi < -1, \\ c_0 - 2c_1 \cos \theta_s, & \phi > 1, \end{cases}$$

with $c_0 > 2|c_1 \cos \theta_s|$. Under such type of modifications, the boundary energy can be bounded from below as well.

3. NUMERICAL SCHEMES

We now construct time marching schemes to solve the NSCH system (2.4)-(2.5)-(2.6)-(2.7) with boundary conditions of GNBC (2.9)-(2.10) and DCLC (2.11)-(2.12). With the aim of constructing schemes that are linear, second order, and unconditionally energy stable, we notice that there are several numerical challenges, including (i) how to decouple the computations of velocity and pressure; (ii) how to discretize $f(\phi)$; (iii) how to discretize $g(\phi)$; and (iv) how to develop proper discretizations for convective and stress terms.

The first difficulty (i) actually has been well studied during the last forty years, e.g., the projection type methods are one of the best ways to solve it (cf. the review in [18] and the references therein). The difficulty (ii) is also well studied recently by two class of methods where one is the nonlinear convex splitting method [12, 48, 57, 64], and the other is the linear stabilization approach [6, 33, 34, 41, 47, 49–54, 56, 67, 68, 76–79]. The convex splitting approach is energy stable, however, it produces nonlinear schemes at most cases, thus the implementations are often complicated and the computational costs are high. The linear stabilization approach introduces purely linear schemes, thus it is easy to implement. But, its stability requests a special property (generalized maximum principle) satisfied by the classical PDE solution and the numerical solution, that is very hard to prove in general. Moreover, the second order scheme developed using the linear stabilization method only possesses the conditional energy stability (cf. the detailed rigorous proof in [51]), i.e., the time step size is controlled by the interfacial thickness.

Therefore, in this paper, we use a newly developed IEQ approach, which has been successfully applied to solve a number of gradient flow type models (cf. [21, 66, 69–73]). Its idea is to make the free energy quadratic in terms of new variables via the change of variables. Then the free energy and the PDE system are transformed into equivalent forms and thus the nonlinear terms can be treated semi-explicitly.

More precisely, we define two new variables

$$(3.1) \quad U = \phi^2 - 1, \quad W = \sqrt{G(\phi) + C},$$

where C is a constant to ensure $G(\phi) + C$ to be positive, for instance, $C = \frac{\sqrt{2}}{3} + \eta$ with any $\eta > 0$. Hence we can rewrite the total free energy to be

$$(3.2) \quad E_{tot}(\mathbf{u}, \phi, U, W) = \int_{\Omega} \left(\frac{1}{2} |\mathbf{u}|^2 + \lambda \left(\frac{\epsilon}{2} |\nabla \phi|^2 + \frac{1}{4\epsilon} U^2 \right) \right) d\mathbf{x} + \lambda \int_{\Gamma} W^2 ds - \lambda C |\Gamma|.$$

Thus, we have a new and an equivalent PDE system as follows

$$(3.3) \quad \phi_t + \nabla \cdot (\mathbf{u}\phi) = M\Delta\mu,$$

$$(3.4) \quad \mu = \lambda(-\epsilon\Delta\phi + \frac{1}{\epsilon}\phi U),$$

$$(3.5) \quad \mathbf{u}_t + (\mathbf{u} \cdot \nabla)\mathbf{u} - \nu\Delta\mathbf{u} + \nabla p + \phi\nabla\mu = 0,$$

$$(3.6) \quad \nabla \cdot \mathbf{u} = 0,$$

$$(3.7) \quad U_t = 2\phi\phi_t,$$

with the GNBC on Γ as

$$(3.8) \quad \mathbf{u} \cdot \mathbf{n} = 0,$$

$$(3.9) \quad \nu\partial_{\mathbf{n}}\mathbf{u}_\tau = -\nu\ell(\phi)(\mathbf{u}_\tau - \mathbf{u}_w) - \frac{\lambda}{\gamma}\dot{\phi}\nabla_\tau\phi,$$

and DCLC as

$$(3.10) \quad \partial_{\mathbf{n}}\mu = 0,$$

$$(3.11) \quad \epsilon\partial_{\mathbf{n}}\phi = -\frac{1}{\gamma}\dot{\phi} - Z(\phi)W,$$

$$(3.12) \quad W_t = \frac{1}{2}Z(\phi)\phi_t,$$

where

$$(3.13) \quad Z(\phi) = \frac{g(\phi)}{\sqrt{G(\phi) + C}}.$$

The initial conditions read as

$$(3.14) \quad \phi|_{t=0} = \phi_0, \quad \mathbf{u}|_{t=0} = \mathbf{u}_0, \quad U|_{t=0} = \phi_0^2 - 1, \quad W|_{t=0} = \sqrt{G(\phi_0) + C}.$$

We derive the energy dissipative law for this new system (3.3)-(3.12) as follows.

Theorem 3.1. *The NSCH system with GNBC and DCLC (3.3)-(3.12) satisfies the following energy dissipation law*

$$(3.15) \quad \begin{aligned} \frac{d}{dt}E_{tot}(\mathbf{u}, \phi, U, W) = & -\nu\|\nabla\mathbf{u}\|^2 - M\|\nabla\mu\|^2 \\ & - \frac{\lambda}{\gamma}\|\dot{\phi}\|_\Gamma^2 - \nu\|\sqrt{\ell(\phi)}\mathbf{u}_s\|_\Gamma^2 - \nu(\ell(\phi)\mathbf{u}_s, \mathbf{u}_w)_\Gamma, \end{aligned}$$

where $E_{tot}(\mathbf{u}, \phi, U, W)$ is defined in (3.2).

Proof. By taking the L^2 inner product of equation (3.3) with μ , and using boundary conditions (3.8) and (3.10), we get

$$(3.16) \quad (\phi_t, \mu) - (\mathbf{u}\phi, \nabla\mu) = -M\|\nabla\mu\|^2.$$

By taking the L^2 inner product of equation (3.4) with $-\phi_t$, we have

$$(3.17) \quad -(\mu, \phi_t) = \lambda(\epsilon\partial_{\mathbf{n}}\phi, \phi_t)_\Gamma - \frac{\lambda\epsilon}{2}\frac{d}{dt}\|\nabla\phi\|^2 - \frac{\lambda}{\epsilon}(\phi U, \phi_t).$$

By taking the L^2 inner product of (3.7) with $\frac{\lambda}{2\epsilon}U$, we obtain

$$(3.18) \quad \lambda\frac{d}{dt}\frac{1}{4\epsilon}\|U\|^2 = \frac{\lambda}{\epsilon}(\phi\phi_t, U).$$

By taking the L^2 inner product of equation (3.5) with \mathbf{u} , using the divergence free condition (3.6), we get

$$(3.19) \quad \frac{d}{dt} \frac{1}{2} \|\mathbf{u}\|^2 = -\nu \|\nabla \mathbf{u}\|^2 + (\nu \partial_{\mathbf{n}} \mathbf{u}_\tau, \mathbf{u}_\tau)_\Gamma - (\phi \nabla \mu, \mathbf{u}).$$

By taking the summation of (3.16)-(3.19), we obtain

$$(3.20) \quad \frac{d}{dt} \left(\frac{1}{2} \|\mathbf{u}\|^2 + \lambda \left(\frac{\epsilon}{2} \|\nabla \phi\|^2 + \frac{1}{4\epsilon} \|U\|^2 \right) \right) = -\nu \|\nabla \mathbf{u}\|^2 - M \|\nabla \mu\|^2 \\ + (\nu \partial_{\mathbf{n}} \mathbf{u}, \mathbf{u})_\Gamma + \lambda (\epsilon \partial_{\mathbf{n}} \phi, \phi_t)_\Gamma.$$

Then, we use boundary condition (3.9) and (3.11), to derive

$$(3.21) \quad \begin{aligned} (\nu \partial_{\mathbf{n}} \mathbf{u}, \mathbf{u})_\Gamma &= (\nu \partial_{\mathbf{n}} \mathbf{u}_\tau, \mathbf{u}_\tau)_\Gamma \\ &= \left(-\frac{\lambda}{\gamma} \dot{\phi} \nabla_\tau \phi - \nu \ell(\phi) (\mathbf{u}_\tau - \mathbf{u}_w), \mathbf{u}_\tau \right)_\Gamma \\ &= -\frac{\lambda}{\gamma} \left(\dot{\phi} \nabla_\tau \phi, \mathbf{u}_\tau \right)_\Gamma - \nu (\ell(\phi) \mathbf{u}_s, \mathbf{u}_s + \mathbf{u}_w)_\Gamma, \end{aligned}$$

and

$$(3.22) \quad \begin{aligned} \lambda (\epsilon \partial_{\mathbf{n}} \phi, \phi_t)_\Gamma &= -\frac{\lambda}{\gamma} (\dot{\phi}, \phi_t)_\Gamma - \lambda (Z(\phi) W, \phi_t)_\Gamma \\ &= -\frac{\lambda}{\gamma} (\dot{\phi}, \dot{\phi} - \mathbf{u}_\tau \cdot \nabla_\tau \phi)_\Gamma - \lambda (Z(\phi) W, \phi_t)_\Gamma \\ &= -\frac{\lambda}{\gamma} \|\dot{\phi}\|_\Gamma^2 + \frac{\lambda}{\gamma} (\dot{\phi}, \mathbf{u}_\tau \cdot \nabla_\tau \phi)_\Gamma - \lambda (Z(\phi) W, \phi_t)_\Gamma. \end{aligned}$$

By taking the L^2 inner product of (3.12) with $2\lambda W$, we obtain

$$(3.23) \quad \lambda \frac{d}{dt} \|W\|_\Gamma^2 = \lambda (Z(\phi) \phi_t, W)_\Gamma.$$

Summing up (3.20), (3.21), (3.22) and (3.23), we get the desired energy law (3.15). \square

Remark 3.1. We consider the nonlinear potential $F(\phi)$ in the bulk part and the interfacial potential $G(\phi)$ as two quadratic functionals by applying appropriate substitutions. Therefore, after simple substitutions using new variables, the energy is transformed to an equivalent quadratic form. We emphasize that the new transformed system (3.3)-(3.12) is exactly equivalent to the original system (2.4)-(2.5)-(2.6)-(2.7), (2.9)-(2.10)-(2.11)-(2.12) that can be easily obtained by integrating (3.7) and (3.12) with respect to the time. Therefore, the energy law (3.15) for the transformed system is exactly the same as the energy law (2.15) for the original system for the time-continuous case. We will develop time-marching schemes for the new transformed system (3.3)-(3.12) that in turn follows the new energy dissipation law (3.15) instead of the energy law (2.14) for the original system.

We fix some notations here. Let $\delta t > 0$ be a time step size and set $t^n = n\delta t$ for $0 \leq n \leq N = [T/\delta t]$. Let S^n denotes the numerical approximation to $S(\cdot, t)|_{t=t^n}$, and $S^{n+\frac{1}{2}} = \frac{S^{n+1} + S^n}{2}$ for any function S . We define two Sobolev space $H_c^1(\Omega) = \{\phi \in H^1(\Omega) : \int_\Omega \phi = 0\}$ and $H_{\mathbf{u}}(\Omega) = \{\mathbf{u} \in [H^1(\Omega)]^d : \mathbf{u} \cdot \mathbf{n}|_\Gamma = 0\}$, provided that Γ is smooth enough.

3.1. Crank-Nicolson Scheme. We first construct a second order Crank-Nicolson scheme (CN2) for the system (3.3)-(3.12), as follows.

Scheme 1. Assuming that $\phi^n, \mathbf{u}^n, p^n, U^n, W^n, \phi^{n-1}, \mathbf{u}^{n-1}$ are given, we compute $\phi^{n+1}, \mathbf{u}^{n+1}, p^{n+1}, U^{n+1}, W^{n+1}$ in two steps.

Step 1: We update $\phi^{n+1}, \mu^{n+\frac{1}{2}}, \tilde{\mathbf{u}}^{n+1}, U^{n+1}, W^{n+1}$ as follows,

$$(3.24) \quad \frac{\phi^{n+1} - \phi^n}{\delta t} + \nabla \cdot (\tilde{\mathbf{u}}^{n+\frac{1}{2}} \phi^{*,n+\frac{1}{2}}) = M \Delta \mu^{n+\frac{1}{2}},$$

$$(3.25) \quad \mu^{n+\frac{1}{2}} = \lambda \left(-\epsilon \Delta \phi^{n+\frac{1}{2}} + \frac{1}{\epsilon} \phi^{*,n+\frac{1}{2}} U^{n+\frac{1}{2}} \right),$$

$$(3.26) \quad U^{n+1} - U^n = 2 \phi^{*,n+\frac{1}{2}} (\phi^{n+1} - \phi^n),$$

$$(3.27) \quad \frac{\tilde{\mathbf{u}}^{n+1} - \mathbf{u}^n}{\delta t} + B(\mathbf{u}^{*,n+\frac{1}{2}}, \tilde{\mathbf{u}}^{n+\frac{1}{2}}) - \nu \Delta \tilde{\mathbf{u}}^{n+\frac{1}{2}} + \nabla p^n + \phi^{*,n+\frac{1}{2}} \nabla \mu^{n+\frac{1}{2}} = 0,$$

with the following boundary conditions on Γ ,

$$(3.28) \quad \tilde{\mathbf{u}}^{n+1} \cdot \mathbf{n} = 0,$$

$$(3.29) \quad \nu \partial_{\mathbf{n}} \tilde{\mathbf{u}}_{\tau}^{n+\frac{1}{2}} = -\nu \ell^{*,n+\frac{1}{2}} (\tilde{\mathbf{u}}^{n+\frac{1}{2}} - \mathbf{u}_w) - \frac{\lambda}{\gamma} \dot{\phi}^{n+\frac{1}{2}} \nabla_{\tau} \phi^{*,n+\frac{1}{2}},$$

$$(3.30) \quad \partial_{\mathbf{n}} \mu^{n+\frac{1}{2}} = 0,$$

$$(3.31) \quad \epsilon \partial_{\mathbf{n}} \phi^{n+\frac{1}{2}} = -\frac{1}{\gamma} \dot{\phi}^{n+\frac{1}{2}} - Z^{*,n+\frac{1}{2}} W^{n+\frac{1}{2}},$$

$$(3.32) \quad W^{n+1} - W^n = \frac{1}{2} Z^{*,n+\frac{1}{2}} (\phi^{n+1} - \phi^n),$$

where

$$(3.33) \quad \begin{cases} B(\mathbf{u}, v) = (\mathbf{u} \cdot \nabla) v + \frac{1}{2} (\nabla \cdot \mathbf{u}) v, \\ \tilde{\mathbf{u}}^{n+\frac{1}{2}} = \frac{\tilde{\mathbf{u}}^{n+1} + \mathbf{u}^n}{2}, \quad \mathbf{u}^{*,n+\frac{1}{2}} = \frac{3}{2} \mathbf{u}^n - \frac{1}{2} \mathbf{u}^{n-1}, \\ \phi^{*,n+\frac{1}{2}} = \frac{3}{2} \phi^n - \frac{1}{2} \phi^{n-1}, \quad Z^{*,n+\frac{1}{2}} = Z(\phi^{*,n+\frac{1}{2}}), \quad \ell^{*,n+\frac{1}{2}} = \ell(\phi^{*,n+\frac{1}{2}}), \\ \dot{\phi}^{n+\frac{1}{2}} = \frac{\phi^{n+1} - \phi^n}{\delta t} + \tilde{\mathbf{u}}_{\tau}^{n+\frac{1}{2}} \cdot \nabla_{\tau} \phi^{*,n+\frac{1}{2}}. \end{cases}$$

Step 2: We update \mathbf{u}^{n+1} and p^{n+1} as follows,

$$(3.34) \quad \frac{\mathbf{u}^{n+1} - \tilde{\mathbf{u}}^{n+1}}{\delta t} + \nabla \left(\frac{p^{n+1} - p^n}{2} \right) = 0,$$

$$(3.35) \quad \nabla \cdot \mathbf{u}^{n+1} = 0,$$

with the boundary condition on Γ ,

$$(3.36) \quad \mathbf{u}^{n+1} \cdot \mathbf{n} = 0.$$

Remark 3.2. The computations of $(\phi^{n+1}, \mu^{n+\frac{1}{2}}, \tilde{\mathbf{u}}^{n+1})$ and the pressure p^{n+1} are totally decoupled via a second order pressure correction scheme [62] and a subtle implicit-explicit treatment for the stress and convective terms. It is quite an open problem on how to develop a second order scheme that can decouple the computations of (ϕ, μ) from the velocity field \mathbf{u} . All decoupled type energy stable schemes were first order accurate in time (cf. [34, 38, 53, 54, 56]). The adopted projection method here was analyzed in [46] where it is shown (discrete time, continuous space) that the schemes is second order accurate for velocity in $\ell^2(0, T; L^2(\Omega))$ but only first order accurate for

pressure in $\ell^\infty(0, T; L^2(\Omega))$. The loss of accuracy for pressure is due to the artificial boundary condition (3.34) imposed on pressure [11]. We refer to [18, 25] and references therein for analysis on this type of discretization.

Schemes (3.24)-(3.32) is totally linear since we handle the convective and stress terms by compositions of implicit (Crank-Nicolson) and explicit (second order extrapolation) discretization at $t^{n+\frac{1}{2}}$. Apparently, the new variables U and W will bring up some extra computational cost. But in fact, we do not need to calculate them explicitly in each step. This is because that we can rewrite (3.26) and (3.32) as follows,

$$(3.37) \quad \begin{cases} \frac{U^{n+1} + U^n}{2} = S^n + \phi^{*,n+\frac{1}{2}}\phi^{n+1}, & S^n = U^n - \phi^{*,n+\frac{1}{2}}\phi^n, \\ \frac{W^{n+1} + W^n}{2} = D^n + \frac{1}{4}Z^{*,n+\frac{1}{2}}\phi^{n+1}, & D^n = W^n - \frac{1}{4}Z^{*,n+\frac{1}{2}}\phi^n. \end{cases}$$

Thus the scheme (3.24)-(3.32) can be written as

$$(3.38) \quad \begin{cases} \phi^{n+1} + \frac{\delta t}{2} \nabla \cdot (\tilde{\mathbf{u}}^{n+1} \phi^{*,n+\frac{1}{2}}) - \delta t M \Delta \mu^{n+\frac{1}{2}} = f_1, \\ -\mu^{n+\frac{1}{2}} - \frac{\lambda \epsilon}{2} \Delta \phi^{n+1} + \frac{\lambda}{\epsilon} (\phi^{*,n+\frac{1}{2}})^2 \phi^{n+1} = f_2, \\ \frac{1}{2} \tilde{\mathbf{u}}^{n+1} + \frac{\delta t}{4} B(\mathbf{u}^{*,n+\frac{1}{2}}, \tilde{\mathbf{u}}^{n+1}) - \frac{\nu \delta t}{4} \Delta \mathbf{u}^{n+1} + \frac{\delta t}{2} \phi^{*,n+\frac{1}{2}} \nabla \mu^{n+\frac{1}{2}} = f_3, \end{cases}$$

with the following boundary conditions on Γ ,

$$(3.39) \quad \begin{cases} \tilde{\mathbf{u}}^{n+1} \cdot \mathbf{n} = 0, \\ \nu \partial_{\mathbf{n}} \tilde{\mathbf{u}}^{n+1} = -\nu \ell^{*,n+\frac{1}{2}} \tilde{\mathbf{u}}^{n+1} - \frac{2\lambda}{\gamma} \phi^{n+1} \nabla \phi^{*,n+\frac{1}{2}} + g_1, \\ \partial_{\mathbf{n}} \mu^{n+\frac{1}{2}} = 0, \\ \epsilon \partial_{\mathbf{n}} \phi^{n+1} = -\frac{2}{\gamma} \phi^{n+1} - \frac{1}{2} (Z^{*,n+\frac{1}{2}})^2 \phi^{n+1} + g_2, \end{cases}$$

where the definition of ϕ^{n+1} is

$$(3.40) \quad \phi^{n+1} = \frac{1}{\delta t} \phi^{n+1} + \frac{1}{2} \tilde{\mathbf{u}}_\tau^{n+1} \cdot \nabla_\tau \phi^{*,n+\frac{1}{2}},$$

and f_1, f_2, f_3, g_1, g_2 include all terms from previous time steps that read as

$$(3.41) \quad \begin{cases} f_1 = -\frac{\delta t}{2} \nabla \cdot (\mathbf{u}^n \phi^{*,n+\frac{1}{2}}) + \phi^n, \\ f_2 = \frac{\lambda \epsilon}{2} \Delta \phi^n - \frac{\lambda}{\epsilon} \phi^{*,n+\frac{1}{2}} S^n, \\ f_3 = \frac{1}{2} \mathbf{u}^n - \frac{\delta t}{4} B(\mathbf{u}^{*,n+\frac{1}{2}}, \mathbf{u}^n) - \frac{\delta t}{2} \nabla p^n + \frac{\nu \delta t}{4} \Delta \mathbf{u}^n, \\ g_1 = -\nu \partial_{\mathbf{n}} \mathbf{u}^n - \nu \ell^{*,n+\frac{1}{2}} (\mathbf{u}^n - 2\mathbf{u}_w) - \frac{2\lambda}{\gamma} \left(-\frac{\phi^n}{\delta t} + \frac{1}{2} \mathbf{u}_\tau^n \cdot \nabla_\tau \phi^{*,n+\frac{1}{2}} \right) \nabla \phi^{*,n+\frac{1}{2}}, \\ g_2 = \frac{2}{\gamma} \left(\frac{\phi^n}{\delta t} - \frac{1}{2} \mathbf{u}_\tau^n \cdot \nabla_\tau \phi^{*,n+\frac{1}{2}} \right) - 2Z^{*,n+\frac{1}{2}} D^n - \epsilon \phi^n. \end{cases}$$

Therefore, we can solve (3.38)-(3.39) directly. Once we obtain $\phi^{n+1}, \mu^{n+\frac{1}{2}}, \tilde{\mathbf{u}}^{n+1}$, the new variables U^{n+1}, W^{n+1} are automatically given in (3.37). In other words, the new variables U, W do not involve any extra computational cost.

By taking the L^2 inner product of (3.24) with 1, we obtain

$$(3.42) \quad \int_{\Omega} \phi^{n+1} d\mathbf{x} = \int_{\Omega} \phi^{n+1} d\mathbf{x} = \dots = \int_{\Omega} \phi^0 d\mathbf{x}.$$

We Let $\bar{\phi} = \frac{1}{|\Omega|} \int_{\Omega} \phi^0 d\mathbf{x}$, $\bar{\mu} = \frac{1}{|\Omega|} \int_{\Omega} \mu d\mathbf{x}$, $\phi = \phi^{n+1} - \bar{\phi}$, $\mu = \mu^{n+\frac{1}{2}} - \bar{\mu}^{n+\frac{1}{2}}$, then the weak form for (3.38)-(3.39) can be written as the following system with unknowns $\mu, \phi \in H_c^1(\Omega)$, $\mathbf{u} \in H_{\mathbf{u}}(\Omega)$,

$$(3.43) \quad (\phi, w) - \frac{\delta t}{2} (\mathbf{u} \phi^{*,n+\frac{1}{2}}, \nabla w) + M \delta t (\nabla \mu, \nabla w) = (f_1, w),$$

$$(3.44) \quad -(\mu, \psi) + \frac{\lambda \epsilon}{2} (\nabla \phi, \nabla \psi) + \frac{\lambda}{\epsilon} ((\phi^{*,n+\frac{1}{2}})^2 \phi, \psi) + \frac{\lambda}{\gamma} (\phi^{\circ}, \psi)_{\Gamma} + \frac{\lambda}{4} ((Z^{*,n+\frac{1}{2}})^2 \phi, \psi)_{\Gamma} = (f_2, \psi) + \frac{\lambda}{2} (g_2, \psi)_{\Gamma},$$

$$(3.45) \quad \frac{1}{2} (\mathbf{u}, \mathbf{v}) + \frac{\delta t}{4} (B(\mathbf{u}^{*,n+\frac{1}{2}}, \mathbf{u}), \mathbf{v}) + \frac{\nu \delta t}{4} (\nabla \mathbf{u}, \nabla \mathbf{v}) + \frac{\delta t}{2} (\phi^{*,n+\frac{1}{2}} \nabla \mu, \mathbf{v}) + \frac{\delta t}{4} (\nu \ell^{*,n+\frac{1}{2}} \mathbf{u}, \mathbf{v})_{\Gamma} + \frac{\lambda}{2\gamma} \delta t (\phi^{\circ} \nabla \phi^{*,n+\frac{1}{2}}, \mathbf{v})_{\Gamma} = (f_3, \mathbf{v}) + \frac{\delta t}{4} (g_1, \mathbf{v})_{\Gamma},$$

for any $w, \psi \in H_c^1(\Omega)$ and $\mathbf{v} \in H_{\mathbf{u}}(\Omega)$, where $\phi^{\circ} = \frac{1}{\delta t} \phi + \frac{1}{2} \mathbf{u}_{\tau} \cdot \nabla_{\tau} \phi^{*,n+\frac{1}{2}}$.

We denote the above linear system (3.43)-(3.45) as

$$(3.46) \quad (\mathbb{A} \mathbf{X}, \mathbf{Y}) = (\mathbb{B}, \mathbf{Y}),$$

where $\mathbf{X} = (\mu, \phi, \mathbf{u})^T$, $\mathbf{Y} = (w, \psi, \mathbf{v})^T$ and $\mathbf{X}, \mathbf{Y} \in (H_c^1, H_c^1, H_{\mathbf{u}})(\Omega)$.

We first show the well-posedness of the above linear system.

Theorem 3.2. *The linear system (3.43)-(3.45) admits a unique solution (μ, ϕ, \mathbf{u}) where $\mu, \phi \in H_c^1(\Omega)$, $\mathbf{u} \in H_{\mathbf{u}}(\Omega)$.*

Proof. (i) For any $\mathbf{X} = (\mu, \phi, \mathbf{u})^T$ and $\mathbf{Y} = (w, \psi, \mathbf{v})^T$ with $\mathbf{X}, \mathbf{Y} \in (H_c^1, H_c^1, H_{\mathbf{u}})(\Omega)$, we have

$$(3.47) \quad (\mathbb{A} \mathbf{X}, \mathbf{Y}) \leq C_1 (\|\phi\|_{H^1} + \|\mu\|_{H^1} + \|\mathbf{u}\|_{H^1}) (\|\psi\|_{H^1} + \|w\|_{H^1} + \|\mathbf{v}\|_{H^1}),$$

from the trace theorem, where $C_1 = C(\delta t, \nu, M, \epsilon, \lambda, \gamma, \|\mathbf{u}^{*,n+\frac{1}{2}}\|_{\infty}, \|\phi^{*,n+\frac{1}{2}}\|_{\infty}, \|Z^{*,n+\frac{1}{2}}\|_{\infty})$. Therefore, the bilinear form $(\mathbb{A} \mathbf{X}, \mathbf{Y})$ is bounded.

(ii) It is easy to derive that

$$(3.48) \quad \begin{aligned} (\mathbb{A} \mathbf{X}, \mathbf{X}) &= \frac{1}{2} \|\mathbf{u}\|^2 + \frac{\nu \delta t}{4} \|\nabla \mathbf{u}\|^2 + \frac{\lambda \epsilon}{2} \|\nabla \phi\|^2 + \frac{\lambda}{\epsilon} \|\phi^{*,n+\frac{1}{2}} \phi\|^2 + M \delta t \|\nabla \mu\|^2 \\ &\quad + \frac{\lambda \delta t}{\gamma} \|\phi^{\circ}\|_{\Gamma}^2 + \frac{\lambda}{4} \|Z^{*,n+\frac{1}{2}} \phi\|_{\Gamma}^2 + \frac{\delta t}{2} \nu \|(\ell^{*,n+\frac{1}{2}})^{\frac{1}{2}} \mathbf{u}_{\tau}\|_{\Gamma}^2 \\ &\geq C_2 (\|\phi\|_{H^1}^2 + \|\mu\|_{H^1}^2 + \|\mathbf{u}\|_{H^1}^2), \end{aligned}$$

from Poincaré inequality (since $\int_{\Omega} \phi d\mathbf{x} = \int_{\Omega} \mu d\mathbf{x} = 0$), where $C_2 = C(\delta t, \nu, M, \epsilon, \lambda)$. Thus the bilinear form $(\mathbb{A} \mathbf{X}, \mathbf{Y})$ is coercive.

Then from the Lax-Milgram theorem, we conclude the linear system (3.46) admits a unique solution $(\mu, \phi, \mathbf{u}) \in (H_c^1, H_c^1, H_{\mathbf{u}})(\Omega)$. Namely, the linear system (3.38)-(3.39) admits a unique solution $(\mu^{n+\frac{1}{2}}, \phi^{n+1}, \tilde{\mathbf{u}}^{n+1})$ in $(H_c^1, H_c^1, H_{\mathbf{u}})(\Omega)$. \square

The stability result of the proposed Crank-Nicolson scheme follows the same lines as in the derivation of the new PDE energy dissipation law Theorem 3.1, as follows.

Theorem 3.3. *The scheme (3.24)-(3.36) is unconditionally energy stable, in the sense that, it satisfies the following discrete energy dissipation law, provided that $\mathbf{u}_w = 0$,*

$$(3.49) \quad \begin{aligned} E_{cn2}^{n+1} = & E_{cn2}^n - M\delta t \|\nabla \mu^{n+\frac{1}{2}}\|^2 - \nu\delta t \|\nabla \tilde{\mathbf{u}}^{n+\frac{1}{2}}\|^2 \\ & - \nu\delta t \|(\ell^{*,n+\frac{1}{2}})^{\frac{1}{2}} \tilde{\mathbf{u}}^{n+\frac{1}{2}}\|_{\Gamma}^2 - \frac{\lambda\delta t}{\gamma} \|\dot{\phi}^{n+\frac{1}{2}}\|_{\Gamma}^2, \end{aligned}$$

where

$$(3.50) \quad E_{cn2}^n = E_{tot}(\mathbf{u}^n, \phi^n, U^n, W^n) + \frac{\delta t^2}{8} \|\nabla p^n\|^2,$$

and $E_{tot}(\mathbf{u}, \phi, U, W)$ is defined in (3.2).

Proof. By taking the L^2 inner product of (3.24) with $\delta t \mu^{n+\frac{1}{2}}$ and performing integration by parts, we obtain

$$(3.51) \quad (\phi^{n+1} - \phi^n, \mu^{n+\frac{1}{2}}) - \delta t (\tilde{\mathbf{u}}^{n+\frac{1}{2}} \phi^{*,n+\frac{1}{2}}, \nabla \mu^{n+\frac{1}{2}}) = -M\delta t \|\nabla \mu^{n+\frac{1}{2}}\|^2.$$

By taking the L^2 inner product of (3.25) with $-(\phi^{n+1} - \phi^n)$, we obtain

$$(3.52) \quad \begin{aligned} -(\mu^{n+\frac{1}{2}}, \phi^{n+1} - \phi^n) = & -\lambda\epsilon \left(\frac{1}{2} \|\nabla \phi^{n+1}\|^2 - \frac{1}{2} \|\nabla \phi^n\|^2 \right) - \frac{\lambda}{\epsilon} (\phi^{*,n+\frac{1}{2}} U^{n+\frac{1}{2}}, \phi^{n+1} - \phi^n) \\ & + \lambda(\epsilon \partial_{\mathbf{n}} \phi^{n+\frac{1}{2}}, \phi^{n+1} - \phi^n)_{\Gamma}. \end{aligned}$$

By taking the L^2 inner product of (3.26) with $\frac{\lambda}{2\epsilon} U^{n+\frac{1}{2}}$, we obtain

$$(3.53) \quad \lambda \left(\frac{\|U^{n+1}\|^2}{4\epsilon} - \frac{\|U^n\|^2}{4\epsilon} \right) = \frac{\lambda}{\epsilon} (\phi^{*,n+\frac{1}{2}} (\phi^{n+1} - \phi^n), U^{n+\frac{1}{2}}).$$

By taking the L^2 inner product of (3.27) with $\delta t \tilde{\mathbf{u}}^{n+\frac{1}{2}}$, we obtain

$$(3.54) \quad \begin{aligned} \frac{1}{2} \|\tilde{\mathbf{u}}^{n+1}\|^2 - \frac{1}{2} \|\mathbf{u}^n\|^2 + \delta t \nu \|\nabla \tilde{\mathbf{u}}^{n+\frac{1}{2}}\|^2 - \delta t (\nu \partial_{\mathbf{n}} \tilde{\mathbf{u}}^{n+\frac{1}{2}}, \tilde{\mathbf{u}}^{n+\frac{1}{2}})_{\Gamma} \\ + \delta t (\nabla p^n, \tilde{\mathbf{u}}^{n+\frac{1}{2}}) + \delta t (\phi^{*,n+\frac{1}{2}} \nabla \mu^{n+\frac{1}{2}}, \tilde{\mathbf{u}}^{n+\frac{1}{2}}) = 0. \end{aligned}$$

By taking the L^2 inner product of (3.34) with $\delta t \mathbf{u}^{n+1}$ and using the divergence free condition for \mathbf{u}^{n+1} from (3.35), we obtain

$$(3.55) \quad \frac{1}{2} (\|\mathbf{u}^{n+1}\|^2 - \|\tilde{\mathbf{u}}^{n+1}\|^2) + \frac{1}{2} \|\mathbf{u}^{n+1} - \tilde{\mathbf{u}}^{n+1}\|^2 = 0.$$

We further rewrite the projection step (3.34) as

$$(3.56) \quad \mathbf{u}^{n+1} + \mathbf{u}^n - 2\tilde{\mathbf{u}}^{n+\frac{1}{2}} + \frac{\delta t}{2} \nabla(p^{n+1} - p^n) = 0.$$

By taking the L^2 inner product of the above equation with $\frac{\delta t}{2} \nabla p^n$ and applying the divergence free condition for $\mathbf{u}^{n+1} + \mathbf{u}^n$, we obtain

$$(3.57) \quad \frac{\delta t^2}{8} (\|\nabla p^{n+1}\|^2 - \|\nabla p^n\|^2 - \|\nabla p^{n+1} - \nabla p^n\|^2) = \delta t (\tilde{\mathbf{u}}^{n+\frac{1}{2}}, \nabla p^n).$$

On the other hand, it follows directly from (3.34) that

$$(3.58) \quad \frac{\delta t^2}{8} \|\nabla(p^{n+1} - p^n)\|^2 = \frac{1}{2} \|\mathbf{u}^{n+1} - \tilde{\mathbf{u}}^{n+1}\|^2.$$

Summing up (3.51), (3.52), (3.53), (3.54), (3.55), (3.57) and (3.58), we obtain

$$\begin{aligned}
(3.59) \quad & \lambda \epsilon \left(\frac{1}{2} \|\nabla \phi^{n+1}\|^2 - \frac{1}{2} \|\nabla \phi^n\|^2 \right) + \lambda \left(\frac{\|U^{n+1}\|^2}{4\epsilon} - \frac{\|U^n\|^2}{4\epsilon} \right) + M \delta t \|\nabla \mu^{n+\frac{1}{2}}\|^2 \\
& + \frac{1}{2} \|\mathbf{u}^{n+1}\|^2 - \frac{1}{2} \|\mathbf{u}^n\|^2 + \nu \delta t \|\nabla \tilde{\mathbf{u}}^{n+\frac{1}{2}}\|^2 + \frac{\delta t^2}{8} (\|\nabla p^{n+1}\|^2 - \|\nabla p^n\|^2) \\
& - \delta t (\nu \partial_{\mathbf{n}} \tilde{\mathbf{u}}^{n+\frac{1}{2}}, \tilde{\mathbf{u}}^{n+\frac{1}{2}})_{\Gamma} - \lambda (\epsilon \partial_{\mathbf{n}} \phi^{n+\frac{1}{2}}, \phi^{n+1} - \phi^n)_{\Gamma} = 0.
\end{aligned}$$

To deal with the boundary integrals, from (3.29), we derive

$$\begin{aligned}
(3.60) \quad & -\delta t (\nu \partial_{\mathbf{n}} \tilde{\mathbf{u}}^{n+\frac{1}{2}}, \tilde{\mathbf{u}}^{n+\frac{1}{2}})_{\Gamma} \\
& = \delta t (\nu \ell^{*,n+\frac{1}{2}} (\tilde{\mathbf{u}}^{n+\frac{1}{2}} - \mathbf{u}_w), \tilde{\mathbf{u}}^{n+\frac{1}{2}})_{\Gamma} + \frac{\lambda \delta t}{\gamma} (\dot{\phi}^{n+\frac{1}{2}} \nabla_{\tau} \phi^{*,n+\frac{1}{2}}, \tilde{\mathbf{u}}^{n+\frac{1}{2}})_{\Gamma}.
\end{aligned}$$

From (3.31), we obtain

$$\begin{aligned}
(3.61) \quad & -\lambda (\epsilon \partial_{\mathbf{n}} \phi^{n+\frac{1}{2}}, \phi^{n+1} - \phi^n)_{\Gamma} \\
& = \lambda \left(\frac{1}{\gamma} \dot{\phi}^{n+\frac{1}{2}}, \phi^{n+1} - \phi^n \right)_{\Gamma} + \lambda (Z^{*,n+\frac{1}{2}} W^{n+\frac{1}{2}}, \phi^{n+1} - \phi^n)_{\Gamma} \\
& = \frac{\lambda \delta t}{\gamma} \|\dot{\phi}^{n+\frac{1}{2}}\|_{\Gamma}^2 - \frac{\lambda \delta t}{\gamma} (\dot{\phi}^{n+\frac{1}{2}}, \tilde{\mathbf{u}}^{n+\frac{1}{2}} \cdot \nabla_{\tau} \phi^{*,n+\frac{1}{2}})_{\Gamma} + \lambda (Z^{*,n+\frac{1}{2}} W^{n+\frac{1}{2}}, \phi^{n+1} - \phi^n)_{\Gamma}.
\end{aligned}$$

By taking the L^2 inner product of (3.32) with $2\lambda W^{n+\frac{1}{2}}$, we obtain

$$(3.62) \quad \lambda (\|W^{n+1}\|_{\Gamma}^2 - \|W^n\|_{\Gamma}^2) = \lambda (Z^{*,n+\frac{1}{2}} (\phi^{n+1} - \phi^n), W^{n+\frac{1}{2}})_{\Gamma}.$$

Finally, we combine (3.59)-(3.62) to obtain

$$\begin{aligned}
(3.63) \quad & \lambda \left(\frac{\epsilon}{2} \|\nabla \phi^{n+1}\|^2 - \frac{\epsilon}{2} \|\nabla \phi^n\|^2 \right) + \lambda \left(\frac{\|U^{n+1}\|^2}{4\epsilon} - \frac{\|U^n\|^2}{4\epsilon} \right) + M \delta t \|\nabla \mu^{n+\frac{1}{2}}\|^2 \\
& + \frac{1}{2} \|\mathbf{u}^{n+1}\|^2 - \frac{1}{2} \|\mathbf{u}^n\|^2 + \nu \delta t \|\nabla \tilde{\mathbf{u}}^{n+\frac{1}{2}}\|^2 + \frac{\delta t^2}{8} (\|\nabla p^{n+1}\|^2 - \|\nabla p^n\|^2) \\
& + \nu \delta t (\ell^{*,n+\frac{1}{2}})^{\frac{1}{2}} \tilde{\mathbf{u}}^{n+\frac{1}{2}}\|_{\Gamma}^2 + \frac{\lambda \delta t}{\gamma} \|\dot{\phi}^{n+\frac{1}{2}}\|_{\Gamma}^2 + \lambda (\|W^{n+1}\|_{\Gamma}^2 - \|W^n\|_{\Gamma}^2) \\
& = \nu \delta t (\ell^{*,n+\frac{1}{2}} \mathbf{u}_w, \tilde{\mathbf{u}}^{n+\frac{1}{2}})_{\Gamma},
\end{aligned}$$

which is exactly (3.49) if we let the wall velocity $\mathbf{u}_w = 0$. \square

The proposed scheme follows the new energy dissipation law (3.15) formally instead of the energy law for the originated system (2.14). In the time-continuous case, the two energy laws are the same. In the time-discrete case, the discrete energy E_{cn2}^n (defined in (3.50)) is a second order approximation to the exact energy $E_{tot}(\mathbf{u}^n, \phi^n)$ (defined in (2.15)), since U^{n+1}, W^{n+1} are second order approximations to $\phi^2 - 1$ and $\sqrt{G(\phi) + C}$, that can be observed from the following facts heuristically. For U^{n+1} , from (3.26), we have

$$(3.64) \quad U^{n+1} - ((\phi^{n+1})^2 - 1) = U^n - ((\phi^n)^2 - 1) + R^{n+1},$$

where $R^{n+1} = O((\phi^{n+1} - \phi^n)(\phi^{n+1} - 2\phi^n + \phi^{n-1}))$. Since $R^k = O(\delta t^3)$ for $0 \leq k \leq n+1$ and $U^0 = (\phi^0)^2 - 1$, by mathematical induction we can easily get

$$(3.65) \quad U^{n+1} = (\phi^{n+1})^2 - 1 + O(\delta t^2).$$

Similar arguments are applicable to W^{n+1} .

Several remarks are in order.

Remark 3.3. *The time discretization for the cubic polynomial term $f(\phi)$ induced from the double well potential has been well-studied in a large quantity of literature, see [6, 12, 21, 22, 33, 34, 41, 47–54, 56, 57, 64, 67, 68, 76–79] and the references therein. For instance, one popular method to obtain second order time marching schemes is the convex splitting approach (cf. [21, 22]) since there exists a natural convex-concave decomposition for the double well potential $F(\phi)(:= \phi^4 - 2\phi^2)$. For the boundary energy $G(\phi)$, since its second order derivative is bounded, it is natural to use the linear stabilization approach, see [16, 17, 56, 74]. Namely, $g(\phi)$ is treated explicitly and an extra linear stabilizer is added to improve the stability. However, since the second order scheme by linear stabilization can only possesses the conditional energy stability [51], the recent available unconditionally energy stable schemes are only first order in time.*

The IEQ approach provides a novel way to handle $f(\phi)$ and $g(\phi)$. Its idea is very simple but quite different from the traditional time marching schemes like fully explicit, implicit or other various Taylor expansions to discretize nonlinear potentials. Through a simple substitution of new variables, the complicated nonlinear potentials are transformed into quadratic forms. We summarize the great advantages of this quadratic transformations as follows: (i) this quadratization method works well for various complex nonlinear terms as long as the corresponding nonlinear potentials are bounded from below; (ii) the complicated nonlinear potential is transferred to a quadratic polynomial form which is much easier to handle; (iii) the derivative of the quadratic polynomial is linear, which provides the fundamental support for linearization method; (iv) the quadratic formulation in terms of new variables can automatically maintain this property of positivity (or bounded from below) of the nonlinear potentials.

Remark 3.4. *When the nonlinear potential is a fourth order polynomial, e.g., the double well potential, the IEQ method is exactly the same as the so-called Lagrange Multiplier method developed in [19]. We remark that the idea of Lagrange Multiplier method only works well for the fourth order polynomial potential (ϕ^4). This is because the nonlinear term ϕ^3 (the derivative of ϕ^4) can be naturally decomposed into a multiplication of two factors: $\lambda(\phi)\phi$ that is the Lagrange multiplier term, and the $\lambda(\phi) = \phi^2$ is then defined as the new auxiliary variable U . However, this method might not succeed for other type potentials. For instance, we notice the Flory-Huggins potential is widely used in two-phase model, see also [5]. The induced nonlinear term is logarithmic type as $\ln(\frac{\phi}{1-\phi})$. If one forcefully rewrites this term as $\lambda(\phi)\phi$, then $\lambda(\phi) = \frac{\ln(\frac{\phi}{1-\phi})}{\phi}$ that is the definition of the new variable U . Obviously, such a form is unworkable for algorithms design. Therefore, we can see that the IEQ approach generalizes the Lagrange Multiplier approach which is for double well potential only, and extends its applicability greatly to a unified framework for general dissipative stiff systems with high nonlinearity. About the application of the IEQ approach to handle other type of nonlinear potentials, we refer to the authors' other work in [21, 66, 69, 70, 72].*

Remark 3.5. *The IEQ approach is more efficient than the nonlinear approach like fully implicit or convex splitting. Let us consider the double well potential case, e.g., $F(\phi) = \phi^4$, then IEQ scheme will generate the linear scheme as $(\phi^n)^2\phi^{n+1}$. The implicit or convex splitting approach will produces the scheme as $(\phi^{n+1})^3$. Therefore, if the Newton iterative method is applied for this term, at each iteration the nonlinear convex splitting approach would yield the same linear operator as IEQ approach. Hence the cost of solving the IEQ scheme is the same as the cost of performing one iteration of Newton method for the implicit/convex splitting approach, provided that the same linear solvers are applied (for instance multi-grid with Gauss-Seidel relaxation).*

3.2. Backward Differentiation Scheme. We further develop another second order scheme that is based on backward differentiation formula with the Adam-Bashforth explicit interpolation (BDF2), that reads as follows.

Scheme 2. Assuming that $(\phi, \mathbf{u}, p, U, W)^{n-1}$ and $(\phi, \mathbf{u}, p, U, W)^n$ are already known, we compute $\phi^{n+1}, \mathbf{u}^{n+1}, p^{n+1}, U^{n+1}, W^{n+1}$ from the following second order temporal semi-discrete system:

Step 1: We update $\phi^{n+1}, \tilde{\mathbf{u}}^{n+1}, U^{n+1}, W^{n+1}$ as follows,

$$(3.66) \quad \frac{3\phi^{n+1} - 4\phi^n + \phi^{n-1}}{2\delta t} + \nabla \cdot (\tilde{\mathbf{u}}^{n+1} \phi^{*,n+1}) = M\Delta\mu^{n+1},$$

$$(3.67) \quad \mu^{n+1} = \lambda \left(-\epsilon \Delta \phi^{n+1} + \frac{1}{\epsilon} \phi^{*,n+1} U^{n+1} \right),$$

$$(3.68) \quad 3U^{n+1} - 4U^n + U^{n-1} = 2\phi^{*,n+1}(3\phi^{n+1} - 4\phi^n + \phi^{n-1}),$$

$$(3.69) \quad \frac{3\tilde{\mathbf{u}}^{n+1} - 4\mathbf{u}^n + \mathbf{u}^{n-1}}{2\delta t} + B(\mathbf{u}^{*,n+1}, \tilde{\mathbf{u}}^{n+1}) - \nu \Delta \tilde{\mathbf{u}}^{n+1} + \nabla p^n + \phi^{*,n+1} \nabla \mu^{n+1} = 0,$$

with the boundary conditions

$$(3.70) \quad \tilde{\mathbf{u}}^{n+1} \cdot \mathbf{n} = 0,$$

$$(3.71) \quad \nu \partial_{\mathbf{n}} \tilde{\mathbf{u}}_{\tau}^{n+1} = -\nu \ell^{*,n+1} (\tilde{\mathbf{u}}^{n+1} - \mathbf{u}_w) - \frac{\lambda}{\gamma} \dot{\phi}^{n+1} \nabla_{\tau} \phi^{*,n+1},$$

$$(3.72) \quad \partial_{\mathbf{n}} \mu^{n+1} = 0,$$

$$(3.73) \quad \epsilon \partial_{\mathbf{n}} \phi^{n+1} = -\frac{1}{\gamma} \dot{\phi}^{n+1} - Z^{*,n+1} W^{n+1},$$

$$(3.74) \quad 3W^{n+1} - 4W^n + W^{n-1} = \frac{1}{2} Z^{*,n+1} (3\phi^{n+1} - 4\phi^n + \phi^{n-1}),$$

where

$$(3.75) \quad \begin{cases} \mathbf{u}^{*,n+1} = 2\mathbf{u}^n - \mathbf{u}^{n-1}, & \phi^{*,n+1} = 2\phi^n - \phi^{n-1}, \\ \ell^{*,n+1} = \ell(\phi^{*,n+1}), & Z^{*,n+1} = Z(\phi^{*,n+1}), \\ \dot{\phi}^{n+1} = \frac{3\phi^{n+1} - 4\phi^n + \phi^{n-1}}{2\delta t} + \tilde{\mathbf{u}}_{\tau}^{n+1} \cdot \nabla_{\tau} \phi^{*,n+1}. \end{cases}$$

Step 2: We update \mathbf{u}^{n+1} and p^{n+1} as follows,

$$(3.76) \quad 3 \frac{\mathbf{u}^{n+1} - \tilde{\mathbf{u}}^{n+1}}{2\delta t} + \nabla(p^{n+1} - p^n) = 0,$$

$$(3.77) \quad \nabla \cdot \mathbf{u}^{n+1} = 0,$$

with the boundary condition

$$(3.78) \quad \mathbf{u}^{n+1} \cdot \mathbf{n} = 0 \quad \text{on } \Gamma.$$

Similar to the Crank-Nicolson scheme (3.24)-(3.32), the BDF2 scheme (3.66)-(3.78) is totally linear. We can rewrite (3.68) and (3.74) as follows,

$$(3.79) \quad \begin{cases} U^{n+1} = R^n + 2\phi^{*,n+1} \phi^{n+1}, & R^n = \frac{4U^n - U^{n-1}}{3} - 2\phi^{*,n+1} \frac{4\phi^n - \phi^{n-1}}{3}, \\ W^{n+1} = Q^n + \frac{1}{2} Z^{*,n+1} \phi^{n+1}, & Q^n = \frac{4W^n - W^{n-1}}{3} - \frac{1}{2} Z^{*,n+1} \frac{4\phi^n - \phi^{n-1}}{3}. \end{cases}$$

Thus the scheme (3.66)-(3.74) can be rewritten as

$$(3.80) \quad \begin{cases} \phi^{n+1} + \frac{2\delta t}{3} \nabla \cdot (\tilde{\mathbf{u}}^{n+1} \phi^{*,n+1}) - \frac{2\delta t}{3} M \Delta \mu^{n+1} = \tilde{f}_1, \\ -\mu^{n+1} - \lambda \epsilon \Delta \phi^{n+1} + \frac{2\lambda}{\epsilon} (\phi^{*,n+1})^2 \phi^{n+1} = \tilde{f}_2, \\ \tilde{\mathbf{u}}^{n+1} + \frac{2\delta t}{3} B(\mathbf{u}^{*,n+1}, \tilde{\mathbf{u}}^{n+1}) - \frac{2\nu\delta t}{3} \Delta \mathbf{u}^{n+1} + \frac{2\delta t}{3} \phi^{*,n+1} \nabla \mu^{n+1} = \tilde{f}_3, \end{cases}$$

with the boundary conditions

$$(3.81) \quad \begin{cases} \tilde{\mathbf{u}}^{n+1} \cdot \mathbf{n} = 0, \\ \nu \partial_{\mathbf{n}} \tilde{\mathbf{u}}^{n+1} = -\nu \ell^{*,n+1} \tilde{\mathbf{u}}^{n+1} - \frac{\lambda}{\gamma} \phi^{\diamond n+1} \nabla \phi^{*,n+1} + \tilde{g}_1, \\ \partial_{\mathbf{n}} \mu^{n+\frac{1}{2}} = 0, \\ \epsilon \partial_{\mathbf{n}} \phi^{n+1} = -\frac{1}{\gamma} \phi^{\diamond n+1} - \frac{1}{2} (Z^{*,n+1})^2 \phi^{n+1} + \tilde{g}_2, \end{cases}$$

where

$$(3.82) \quad \begin{cases} \phi^{\diamond n+1} = \frac{3}{2\delta t} \phi^{n+1} + \tilde{\mathbf{u}}^{n+1} \cdot \nabla_{\tau} \phi^{*,n+1}, \\ \tilde{f}_1 = \frac{4\phi^n - \phi^{n-1}}{3}, \\ \tilde{f}_2 = -\frac{\lambda}{\epsilon} \phi^{*,n+1} R^n, \\ \tilde{f}_3 = \frac{4\mathbf{u}^n - \mathbf{u}^{n-1}}{3} - \frac{2\delta t}{3} \nabla p^n, \\ \tilde{g}_1 = \frac{\lambda}{\gamma} \frac{4\phi^n - \phi^{n-1}}{2\delta t} \nabla \phi^{*,n+1} + \nu \ell^{*,n+1} \mathbf{u}_w, \\ \tilde{g}_2 = \frac{1}{\gamma} \frac{4\phi^n - \phi^{n-1}}{2\delta t} - Z^{*,n+1} Q^n. \end{cases}$$

Therefore, we can solve (3.80)-(3.81) directly. Once we obtain $\phi^{n+1}, \mu^{n+\frac{1}{2}}, \tilde{\mathbf{u}}^{n+1}, U^{n+1}, W^{n+1}$ are automatically given in (3.79). Namely, the new variables U, W do not involve any extra computational cost.

Theorem 3.4. *The weak form of the linear system (3.80)-(3.81) admits a unique solution $(\mu^{n+1}, \phi^{n+1}, \tilde{\mathbf{u}}^{n+1})$ where $\mu^{n+1}, \phi^{n+1} \in H_c^1(\Omega)$, and $\tilde{\mathbf{u}}^{n+1} \in H_{\mathbf{u}}(\Omega)$.*

Proof. The proof is similar to Theorem 3.2, thus we omit the details here. \square

Theorem 3.5. *The scheme (3.66)-(3.78) is unconditionally energy stable satisfying the following discrete energy dissipation law, provided $\mathbf{u}_w = 0$,*

$$(3.83) \quad \begin{aligned} E_{bdf}^{n+1} &\leq E_{bdf}^n - M\delta t \|\nabla \mu^{n+1}\|^2 - \nu\delta t \|\nabla \tilde{\mathbf{u}}^{n+1}\|^2 \\ &\quad - \frac{\lambda}{\gamma} \delta t \|\dot{\phi}^{n+1}\|_{\Gamma}^2 - \nu\delta t \|(\ell^{*,n+1})^{\frac{1}{2}} \tilde{\mathbf{u}}^{n+1}\|_{\Gamma}^2, \end{aligned}$$

where

$$\begin{aligned}
 E_{bdf2}^{n+1} = & \frac{1}{2} \left(\frac{\|\mathbf{u}^{n+1}\|^2}{2} + \frac{\|2\mathbf{u}^{n+1} - \mathbf{u}^n\|^2}{2} \right) \\
 (3.84) \quad & + \lambda \left(\frac{\epsilon}{2} \left(\frac{\|\nabla \phi^{n+1}\|^2}{2} + \frac{\|2\nabla \phi^{n+1} - \nabla \phi^n\|^2}{2} \right) + \frac{1}{2} \left(\frac{\|U^{n+1}\|^2}{4\epsilon} + \frac{\|2U^{n+1} - U^n\|^2}{4\epsilon} \right) \right. \\
 & \left. + \left(\frac{\|W^{n+1}\|_{\Gamma}^2}{2} + \frac{\|2W^{n+1} - W^n\|_{\Gamma}^2}{2} \right) \right) + \frac{\delta t^2}{3} \|\nabla p^{n+1}\|^2.
 \end{aligned}$$

Proof. By taking the L^2 inner product of (3.66) with $2\delta t \mu^{n+1}$ and performing integration by parts, we obtain

$$(3.85) \quad (3\phi^{n+1} - 4\phi^n + \phi^{n-1}, \mu^{n+1}) - 2\delta t (\tilde{\mathbf{u}}^{n+1} \phi^{*,n+1}, \nabla \mu^{n+1}) = -2M\delta t \|\nabla \mu^{n+1}\|^2.$$

By taking the L^2 inner product of (3.67) with $-(3\phi^{n+1} - 4\phi^n + \phi^{n-1})$, we obtain

$$\begin{aligned}
 (3.86) \quad & -(\mu^{n+1}, 3\phi^{n+1} - 4\phi^n + \phi^{n-1}) \\
 & = -\frac{\lambda\epsilon}{2} \left(\|\nabla \phi^{n+1}\|^2 - \|\nabla \phi^n\|^2 + \|2\nabla \phi^{n+1} - \nabla \phi^n\|^2 - \|2\nabla \phi^n - \nabla \phi^{n-1}\|^2 \right. \\
 & \quad \left. + \|\nabla(\phi^{n+1} - 2\phi^n + \phi^{n-1})\|^2 \right) \\
 & \quad + \lambda(\epsilon \partial_{\mathbf{n}} \phi^{n+1}, 3\phi^{n+1} - 4\phi^n + \phi^{n-1})_{\Gamma} - \frac{\lambda}{\epsilon} (\phi^{*,n+1} U^{n+1}, 3\phi^{n+1} - 4\phi^n + \phi^{n-1}).
 \end{aligned}$$

By taking the L^2 inner product of (3.68) with $\frac{\lambda}{2\epsilon} U^{n+1}$, we obtain

$$\begin{aligned}
 (3.87) \quad & \frac{\lambda}{4\epsilon} \left(\|U^{n+1}\|^2 - \|U^n\|^2 + \|2U^{n+1} - U^n\|^2 - \|2U^n - U^{n-1}\|^2 + \|U^{n+1} - 2U^n + U^{n-1}\|^2 \right) \\
 & = \frac{\lambda}{\epsilon} (\phi^{*,n+1} (3\phi^{n+1} - 4\phi^n + \phi^{n-1}), U^{n+1}).
 \end{aligned}$$

By taking the L^2 inner product of (3.69) with $2\delta t \tilde{\mathbf{u}}^{n+1}$, we obtain

$$\begin{aligned}
 (3.88) \quad & (3\tilde{\mathbf{u}}^{n+1} - 4\mathbf{u}^n + \mathbf{u}^{n-1}, \tilde{\mathbf{u}}^{n+1}) + 2\nu\delta t \|\nabla \tilde{\mathbf{u}}^{n+1}\|^2 - 2\nu\delta t (\partial_{\mathbf{n}} \tilde{\mathbf{u}}^{n+1}, \tilde{\mathbf{u}}^{n+1})_{\Gamma} \\
 & + 2\delta t (\nabla p^n, \tilde{\mathbf{u}}^{n+1}) + 2\delta t (\phi^{*,n+1} \nabla \mu^{n+1}, \tilde{\mathbf{u}}^{n+1}) = 0.
 \end{aligned}$$

From (3.76), for any function \mathbf{v} with $\nabla \cdot \mathbf{v} = 0$, we can derive

$$(3.89) \quad (\mathbf{u}^{n+1}, \mathbf{v}) = (\tilde{\mathbf{u}}^{n+1}, \mathbf{v}).$$

Then for the first term in (3.88), we have

$$\begin{aligned}
 (3.90) \quad & (3\tilde{\mathbf{u}}^{n+1} - 4\mathbf{u}^n + \mathbf{u}^{n-1}, \tilde{\mathbf{u}}^{n+1}) \\
 & = 3(\tilde{\mathbf{u}}^{n+1} - \mathbf{u}^{n+1}, \tilde{\mathbf{u}}^{n+1} + \mathbf{u}^{n+1}) + (3\mathbf{u}^{n+1} - 4\mathbf{u}^n + \mathbf{u}^{n-1}, \mathbf{u}^{n+1}) \\
 & = 3(\|\tilde{\mathbf{u}}^{n+1}\|^2 - \|\mathbf{u}^{n+1}\|^2) + \frac{1}{2} \left(\|\mathbf{u}^{n+1}\|^2 - \|\mathbf{u}^n\|^2 + \|2\mathbf{u}^{n+1} - \mathbf{u}^n\|^2 \right. \\
 & \quad \left. - \|2\mathbf{u}^n - \mathbf{u}^{n-1}\|^2 + \|\mathbf{u}^{n+1} - 2\mathbf{u}^n + \mathbf{u}^{n-1}\|^2 \right).
 \end{aligned}$$

For the projection step, we rewrite (3.76) as

$$(3.91) \quad \frac{3}{2\delta t} \mathbf{u}^{n+1} + \nabla p^{n+1} = \frac{3}{2\delta t} \tilde{\mathbf{u}}^{n+1} + \nabla p^n.$$

By squaring both sides of the above equality, we obtain

$$(3.92) \quad \frac{9}{4\delta t^2} \|\mathbf{u}^{n+1}\|^2 + \|\nabla p^{n+1}\|^2 = \frac{9}{4\delta t^2} \|\tilde{\mathbf{u}}^{n+1}\|^2 + \|\nabla p^n\|^2 + \frac{3}{\delta t} (\tilde{\mathbf{u}}^{n+1}, \nabla p^n),$$

namely, we have

$$(3.93) \quad \frac{3}{2} (\|\mathbf{u}^{n+1}\|^2 - \|\tilde{\mathbf{u}}^{n+1}\|^2) + \frac{2\delta t^2}{3} (\|\nabla p^{n+1}\|^2 - \|\nabla p^n\|^2) = 2\delta t (\tilde{\mathbf{u}}^{n+1}, \nabla p^n).$$

By taking the L^2 inner product of (3.76) with $2\delta t \mathbf{u}^{n+1}$, we have

$$(3.94) \quad \frac{3}{2} (\|\mathbf{u}^{n+1}\|^2 - \|\tilde{\mathbf{u}}^{n+1}\|^2 + \|\mathbf{u}^{n+1} - \tilde{\mathbf{u}}^{n+1}\|^2) = 0.$$

By combining (3.85)-(3.90) and (3.93)-(3.94), we obtain

$$(3.95) \quad \begin{aligned} & 2M\delta t \|\nabla \mu^{n+1}\|^2 + \frac{3}{2} \|\mathbf{u}^{n+1} - \tilde{\mathbf{u}}^{n+1}\|^2 \\ & + \frac{2\delta t^2}{3} (\|\nabla p^{n+1}\|^2 - \|\nabla p^n\|^2) + 2\nu\delta t \|\nabla \tilde{\mathbf{u}}^{n+1}\|^2 \\ & + \frac{\lambda\epsilon}{2} \left(\|\nabla \phi^{n+1}\|^2 - \|\nabla \phi^n\|^2 + \|2\nabla \phi^{n+1} - \nabla \phi^n\|^2 - \|2\nabla \phi^n - \nabla \phi^{n-1}\|^2 \right. \\ & \quad \left. + \|\nabla \phi^{n+1} - 2\nabla \phi^n + \nabla \phi^{n-1}\|^2 \right) \\ & + \frac{\lambda}{4\epsilon} \left(\|U^{n+1}\|^2 - \|U^n\|^2 + \|2U^{n+1} - U^n\|^2 - \|2U^n - U^{n-1}\|^2 \right. \\ & \quad \left. + \|U^{n+1} - 2U^n + U^{n-1}\|^2 \right) \\ & + \frac{1}{2} \left(\|\mathbf{u}^{n+1}\|^2 - \|\mathbf{u}^n\|^2 + \|2\mathbf{u}^{n+1} - \mathbf{u}^n\|^2 - \|2\mathbf{u}^n - \mathbf{u}^{n-1}\|^2 \right. \\ & \quad \left. + \|\mathbf{u}^{n+1} - 2\mathbf{u}^n + \mathbf{u}^{n-1}\|^2 \right) \\ & - \lambda(\epsilon \partial_{\mathbf{n}} \phi^{n+1}, 3\phi^{n+1} - 4\phi^n + \phi^{n-1})_{\Gamma} - 2\delta t (\nu \partial_{\mathbf{n}} \tilde{\mathbf{u}}^{n+1}, \tilde{\mathbf{u}}^{n+1})_{\Gamma} = 0. \end{aligned}$$

From (3.73), we obtain

$$(3.96) \quad \begin{aligned} & -\lambda \left(\epsilon \partial_{\mathbf{n}} \phi^{n+1}, 3\phi^{n+1} - 4\phi^n + \phi^{n-1} \right)_{\Gamma} \\ & = -\lambda \left(-\frac{1}{\gamma} \dot{\phi}^{n+1} - Z^{*,n+1} W^{n+1}, 3\phi^{n+1} - 4\phi^n + \phi^{n-1} \right)_{\Gamma} \\ & = 2\delta t \frac{\lambda}{\gamma} \|\dot{\phi}^{n+1}\|_{\Gamma}^2 - 2\delta t \frac{\lambda}{\gamma} (\dot{\phi}^{n+1}, \tilde{\mathbf{u}}^{n+1} \cdot \nabla \phi^{*,n+1})_{\Gamma} \\ & \quad + \lambda (Z^{*,n+1} W^{n+1}, 3\phi^{n+1} - 4\phi^n + \phi^{n-1})_{\Gamma}. \end{aligned}$$

From (3.71), we obtain

$$(3.97) \quad \begin{aligned} -2\delta t (\nu \partial_{\mathbf{n}} \tilde{\mathbf{u}}^{n+1}, \tilde{\mathbf{u}}^{n+1})_{\Gamma} & = -2\delta t \left(-\nu \ell^{*,n+1} (\tilde{\mathbf{u}}^{n+1} - \mathbf{u}_w) - \frac{\lambda}{\gamma} \dot{\phi}^{n+1} \nabla \phi^{*,n+1}, \tilde{\mathbf{u}}^{n+1} \right)_{\Gamma} \\ & = 2\delta t \nu \left(\ell^{*,n+1} (\tilde{\mathbf{u}}^{n+1} - \mathbf{u}_w), \tilde{\mathbf{u}}^{n+1} \right)_{\Gamma} + 2\delta t \frac{\lambda}{\gamma} \left(\dot{\phi}^{n+1} \nabla \phi^{*,n+1}, \tilde{\mathbf{u}}^{n+1} \right)_{\Gamma}. \end{aligned}$$

By taking the L^2 inner product of (3.74) with $2\lambda W^{n+1}$, we obtain

$$(3.98) \quad \begin{aligned} & \lambda(\|W^{n+1}\|_{\Gamma}^2 - \|W^n\|_{\Gamma}^2 + \|2W^{n+1} - W^n\|_{\Gamma}^2 - \|2W^n - W^{n-1}\|_{\Gamma}^2 + \|W^{n+1} - 2W^n + W^{n-1}\|_{\Gamma}^2) \\ & = \lambda(Z^{\star, n+1}(3W^{n+1} - 4W^n + W^{n-1}), W^{n+1})_{\Gamma}. \end{aligned}$$

By combining (3.95), (3.96)-(3.98), we obtain

$$\begin{aligned} & 2M\delta t \|\nabla \mu^{n+1}\|^2 + \frac{3}{2} \|\mathbf{u}^{n+1} - \tilde{\mathbf{u}}^{n+1}\|^2 + \frac{2\delta t^2}{3} (\|\nabla p^{n+1}\|^2 - \|\nabla p^n\|^2) + 2\nu\delta t \|\nabla \tilde{\mathbf{u}}^{n+1}\|^2 \\ & + \frac{\lambda\epsilon}{2} (\|\nabla \phi^{n+1}\|^2 - \|\nabla \phi^n\|^2 + \|2\nabla \phi^{n+1} - \nabla \phi^n\|^2 - \|2\nabla \phi^n - \nabla \phi^{n-1}\|^2 + \|\nabla \phi^{n+1} - 2\nabla \phi^n + \nabla \phi^{n-1}\|^2) \\ & + \frac{\lambda}{4\epsilon} (\|U^{n+1}\|^2 - \|U^n\|^2 + \|2U^{n+1} - U^n\|^2 - \|2U^n - U^{n-1}\|^2 + \|U^{n+1} - 2U^n + U^{n-1}\|^2) \\ & + \frac{1}{2} (\|\mathbf{u}^{n+1}\|^2 - \|\mathbf{u}^n\|^2 + \|2\mathbf{u}^{n+1} - \mathbf{u}^n\|^2 - \|2\mathbf{u}^n - \mathbf{u}^{n-1}\|^2 + \|\mathbf{u}^{n+1} - 2\mathbf{u}^n + \mathbf{u}^{n-1}\|^2) \\ & + \lambda(\|W^{n+1}\|_{\Gamma}^2 - \|W^n\|_{\Gamma}^2 + \|2W^{n+1} - W^n\|_{\Gamma}^2 - \|2W^n - W^{n-1}\|_{\Gamma}^2 + \|W^{n+1} - 2W^n + W^{n-1}\|_{\Gamma}^2) \\ & + 2\delta t \frac{\lambda}{\gamma} \|\dot{\phi}^{n+1}\|_{\Gamma}^2 + 2\delta t \nu \|(\ell^{\star, n+1})^{\frac{1}{2}} \tilde{\mathbf{u}}^{n+1}\|_{\Gamma}^2 - 2\delta t \nu (\ell^{\star, n+1} \mathbf{u}_w, \tilde{\mathbf{u}}^{n+1})_{\Gamma} = 0. \end{aligned}$$

Therefore, we conclude the theorem after dropping some positive terms and taking $\mathbf{u}_w = 0$. \square

Remark 3.6. From formal Taylor expansion, we can find

$$(3.99) \quad \begin{aligned} & \left(\frac{\|S^{n+1}\|^2 + \|2S^{n+1} - S^n\|^2}{2\delta t} \right) - \left(\frac{\|S^n\|^2 + \|2S^n - S^{n-1}\|^2}{2\delta t} \right) \\ & \cong \left(\frac{\|S^{n+2}\|^2 - \|S^n\|^2}{2\delta t} \right) + O(\delta t^2) \cong \frac{d}{dt} \|S(t^{n+1})\|^2 + O(\delta t^2), \end{aligned}$$

and

$$(3.100) \quad \frac{\|S^{n+1} - 2S^n + S^{n-1}\|^2}{\delta t} \cong O(\delta t^3)$$

for any variable S . Therefore, the discrete energy law (3.83) is a second order approximation of Theorem 3.1.

4. SPATIAL DISCRETIZATION AND IMPLEMENTATION

We implement a spectral Galerkin method for a 2-dimensional rectangular domain $\Omega = [0, L_x] \times [-1, 1]$ to test the stability and accuracy of the linear schemes proposed in last section. Note that any spatial discretization based on weak formulation and Galerkin approximation of the NSCH coupled system will keep the energy dissipation properties obtained for the temporal semi-discretized schemes. Thus the finite element or spectral element methods can be used as well in a similar way.

Now we take the weak form for the Crank-Nicolson system (3.43)-(3.45) as an example to illustrate the spatial discretization, and the BDF2 scheme can be handled similarly. We obtain a Galerkin approximation by providing appropriate finite dimensional spaces $H_{\mathbf{u}}^N, H_{\mu}^N, H_{\phi}^N$ for $H_{\mathbf{u}}(\Omega), H_c^1(\Omega), H_c^1(\Omega)$ for the velocity field \mathbf{u} , the chemical potential μ and the phase variable ϕ , respectively.

4.1. A Spectral Galerkin Approximation. We assume the system in x direction is periodic, only the top and bottom boundaries ($y = \pm 1$) take the GNBC and DCLC.

We use

$$(4.1) \quad F_m := \text{span}\{E_k(x) = e^{ikx/L_x}, |k| \leq m\}, \quad P_n := \text{span}\{\varphi_k : 0 \leq k \leq n\}$$

as the basis set for x direction and y direction correspondingly, where

$$(4.2) \quad \varphi_0(y) = 1, \quad \varphi_1(y) = x, \quad \varphi_k(y) = L_k(y) - L_{k-2}(y), \quad k = 2, 3, \dots,$$

and $L_k(y)$ denote the Legendre polynomial of degree k . For given m and n , we take $H_\mu^N = H_\phi^N = F_m \otimes P_n$ as the approximation space for μ and ϕ . For the Navier-Stokes equation, the velocity in x -component satisfies the GNBC, the Robin type boundary condition, while the component in y direction satisfies the Dirichlet boundary condition. The Robin type boundary condition is treated naturally in the weak form, the Dirichlet boundary condition is imposed on the approximation space. So we take the Galerkin approximation space for \mathbf{u} as $H_{\mathbf{u}}^N = (F_m \otimes P_n) \times (F_m \otimes P_n^0)$ where $P_n^0 = \text{span}\{\varphi_k, k = 2, \dots, n\}$. The approximation space for pressure is $H_p^N = F_m \otimes P_n \setminus (E_0 \otimes \{P_0, P_n\}) := \left\{ p = \sum_{|k| \leq m, 0 \leq j \leq n} \hat{p}_{kj} E_k(x) \varphi_j(y) : \hat{p}_{00} - \hat{p}_{02} = 0, \hat{p}_{0n} = 0 \right\}$.

4.2. Solution Procedure. By using spectral bases (4.1), the constant-coefficient terms in equations all lead to sparse matrices that is time independent. However, the variable-coefficient terms leads to time-dependent dense matrices, thus explicitly building those time-dependent dense matrices are extremely expensive (Note that, if one use finite element methods, the corresponding matrices will be sparse but time-dependent). So we use a conjugate gradient type solver with preconditioning (PCG), that does not need explicitly building the matrix. Instead, it only needs a subroutine to calculate the matrix-vector product. Since the linear systems are not symmetric, we use BiCGSTAB method. A linear system corresponding to the system (3.43)-(3.45) with \mathbf{u} term in (3.43) removed, which can be efficiently inverted, is taken as a preconditioner. Its effectiveness of this preconditioner is shown in the next section. The solution procedure for the BDF2 scheme is similar.

4.3. The Startup Step. Both CN2 and BDF2 schemes need two initial steps to startup. We can use any first order scheme to calculate $\phi^1, \mathbf{u}^1, p^1, U^1, W^1$. In our simulations, following first order scheme is used. We call it BDF1 scheme.

Step 1: Given $\phi^n, \tilde{\mathbf{u}}^n, p^n, U^n, W^n$, We solve for $\phi^{n+1}, \tilde{\mathbf{u}}^{n+1}, U^{n+1}, W^{n+1}$ from

$$(4.3) \quad \frac{\phi^{n+1} - \phi^n}{\delta t} + \nabla \cdot (\tilde{\mathbf{u}}^{n+1} \phi^n) = M \Delta \mu^{n+1},$$

$$(4.4) \quad \mu^{n+1} = \lambda \left(-\epsilon \Delta \phi^{n+1} + \frac{1}{\epsilon} \phi^n U^{n+1} \right),$$

$$(4.5) \quad U^{n+1} - U^n = 2\phi^n (\phi^{n+1} - \phi^n),$$

$$(4.6) \quad \frac{\tilde{\mathbf{u}}^{n+1} - \mathbf{u}^n}{\delta t} + B(\mathbf{u}^n, \tilde{\mathbf{u}}^{n+1}) - \nu \Delta \tilde{\mathbf{u}}^{n+1} + \nabla p^n + \phi^n \nabla \mu^{n+1} = 0,$$

with the boundary conditions

$$(4.7) \quad \left\{ \begin{array}{l} \tilde{\mathbf{u}}^{n+1} \cdot \mathbf{n} = 0, \\ \nu \partial_{\mathbf{n}} \tilde{\mathbf{u}}_{\tau}^{n+1} = -\nu \ell^n (\tilde{\mathbf{u}}^{n+1} - \mathbf{u}_w) - \frac{\lambda}{\gamma} \dot{\phi}^{n+1} \nabla_{\tau} \phi^n, \\ \partial_{\mathbf{n}} \mu^{n+1} = 0, \\ \epsilon \partial_{\mathbf{n}} \phi^{n+1} = -\frac{1}{\gamma} \dot{\phi}^{n+1} - Z^n W^{n+1}, \\ W^{n+1} - W^n = \frac{1}{2} Z^n (\phi^{n+1} - \phi^n), \end{array} \right.$$

where

$$\dot{\phi}^{n+1} = \frac{\phi^{n+1} - \phi^n}{\delta t} + \tilde{\mathbf{u}}_\tau^{n+1} \cdot \nabla_\tau \phi^n.$$

Step 2: We update \mathbf{u}^{n+1} and p^{n+1} using

$$(4.8) \quad \frac{\mathbf{u}^{n+1} - \tilde{\mathbf{u}}^{n+1}}{\delta t} + \nabla(p^{n+1} - p^n) = 0,$$

$$(4.9) \quad \nabla \cdot \mathbf{u}^{n+1} = 0,$$

with the boundary condition

$$(4.10) \quad \mathbf{u}^{n+1} \cdot \mathbf{n} = 0 \quad \text{on } \Gamma.$$

5. NUMERICAL SIMULATIONS

In this section, we present various numerical experiments to validate the developed schemes (3.24)-(3.36) (denoted by CN2) and (3.66)-(3.78) (denoted by BDF2), and demonstrate their stability and accuracy.

5.1. Basic Scheme Validation. We now examine the accuracy, stability and efficiency of the proposed schemes by performing a classical shear flow experiment between two parallel plates which move in opposite directions at a constant speed. The computed domain is $\Omega = [0, L_x] \times [-1, 1]$. If not explicit specified, the model parameters take default values given below, which is consistent to the benchmark simulation in [16, 17, 42, 44, 56, 74].

$$(5.1) \quad \lambda = 20, \quad M = 0.0125, \quad \gamma = 100, \quad \ell(\phi) = 1/0.19, \quad \nu = 1/0.6, \quad \epsilon = 0.05.$$

5.1.1. Convergence test for space and time. We first test the convergence in space and time by presenting numerical results for two cases. In case 1, we set $\mathbf{u}_w = (\pm 0.7, 0)$, $\theta_s = 64^\circ$, where \mathbf{u}_w is the velocities of upper and bottom plates. the sign of “ \pm ” means the values on top and bottom boundaries have different directions, i.e., the top plate ($y = 1$) moves at the speed 0.7 and the bottom plate ($y = -1$) moves at the speed -0.7 . In case 2, we set $\mathbf{u}_w = (\pm 0.2, 0)$ and $\theta_s = 77.6^\circ$. In both cases, $L_x = 10$ and the initial velocity field takes the profile of Couette flow, while the initial value of ϕ is given as

$$(5.2) \quad \phi_0(x, y) = \tanh \left(\frac{1}{\sqrt{2}\epsilon} (0.25L_x - |x - 0.5L_x|) \right).$$

We use $n_x = 2m + 1$ to denote the number of Fourier modes used in x -direction, $n_y = n + 1$ denote the number of Legendre polynomials used in y -direction (m, n are used in (4.1)). In Fig. 1, we plot the contours of the phase variable ϕ at $t = 5$ for the two cases, that are obtained using the BDF2 scheme with $n_x = 257$, $n_y = 32$, and $\delta t = 0.01$. We only show the results of the BDF2 scheme since the CN2 scheme gives identical results. In Fig. 2, we show the velocity field $\mathbf{u} = (u, v)$ and pressure p for case 2 using the BDF2 scheme. These results are quantitatively consistent to the numerical results obtained in [56]. In Fig. 3, we plot the x -component of velocity at lower boundary $y = -1$ for two different time steps $\delta t = 0.005$ and $\delta t = 0.01$ obtained from the BDF2 scheme and CN2 scheme for the case 2 at $t = 10$. We observe that the results obtained by two schemes are almost identical, which means the time step $\delta t = 0.01$ is small enough to provide very accurate results for this test case.

To test the convergence for spatial discretization, we use a tiny time step $\delta t = 0.0005$ so that the errors from the temporal discretization are negligible compared with the spatial discretization errors. In Fig. 4(a), to test the convergence in x -direction, we fix the number of Legendre modes $n_y = 64$ and vary the number of Fourier modes n_x starting from 41 with the increment 40. The

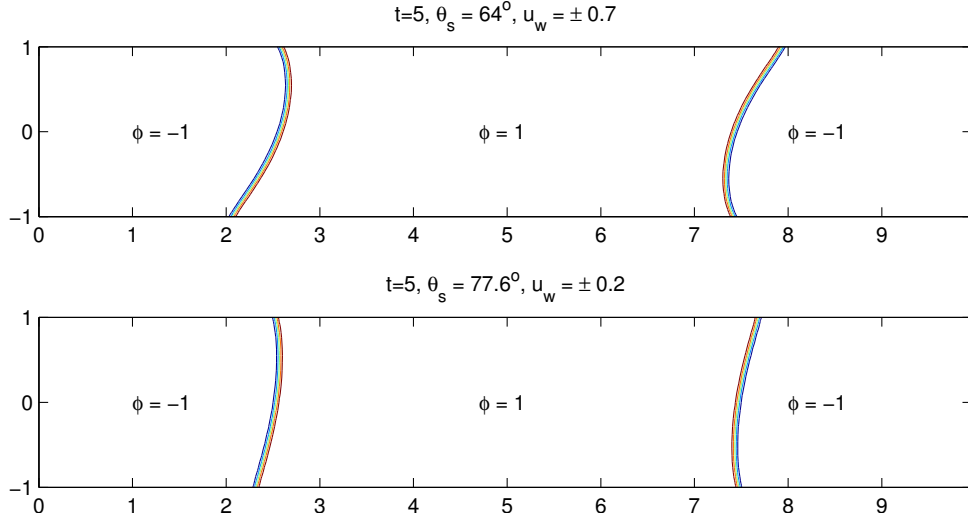


FIG. 1. The contours of phase variable ϕ at $t = 5$ that are obtained by the BDF2 scheme with 257 Fourier modes, 32 Legendre modes and $\delta t = 0.01$. (Top) The contour of ϕ for the case $\mathbf{u}_w = (\pm 0.7, 0)$, $\theta_s = 64^\circ$; (Bottom) The contour of ϕ for the case $\mathbf{u}_w = (\pm 0.2, 0)$, $\theta_s = 77.6^\circ$.

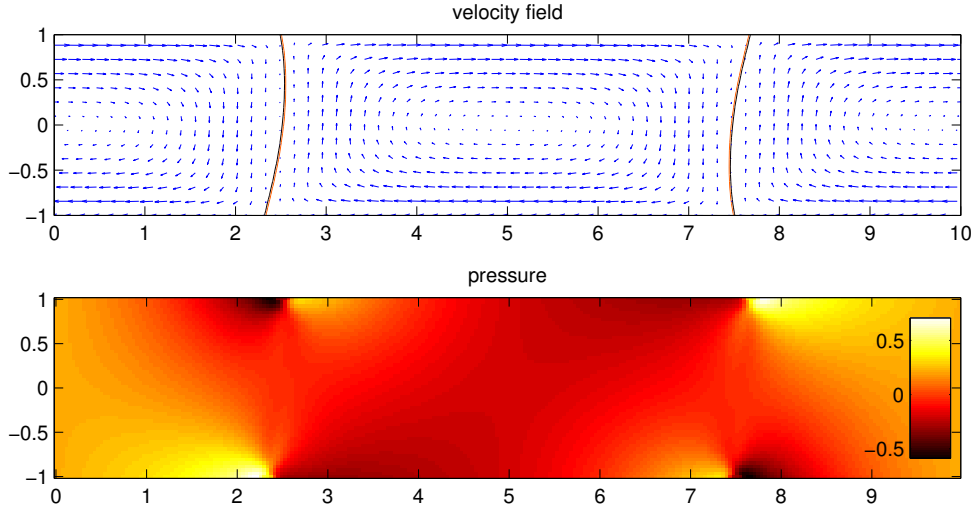


FIG. 2. The information of $\mathbf{u} = (u, v)$, ϕ , p at $t = 5$ obtained from the BDF2 scheme using 257 Fourier modes, 32 Legendre modes and $\delta t = 0.01$ for the case $\theta_s = 77.6^\circ$, $\mathbf{u}_w = (\pm 0.2, 0)$. Other equation parameters are given in (5.1). In the top picture, two solid curves (red) are the interfaces of two phases (where $\phi = 0$), arrows (blue) denote the directions and strength of the velocity at corresponding spatial points. In the bottom picture, color denotes the value of pressure. In both pictures, the horizontal axis is x , vertical axis is y .

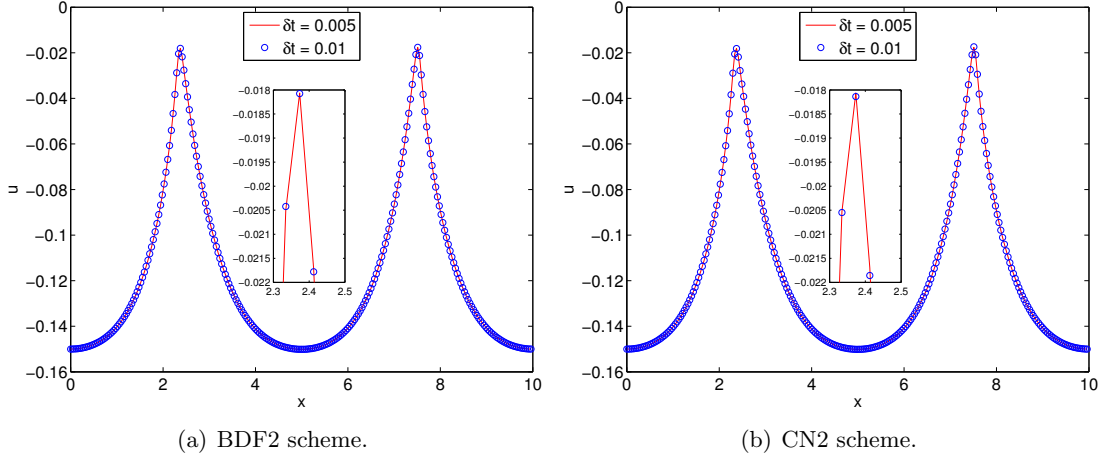


FIG. 3. The x -component velocity at $y = -1, t = 10$ using (a) the BDF2 scheme and (b) the CN2 scheme with $\delta t = 0.005$ and $\delta t = 0.01$ for the case $\theta_s = 77.6^\circ, \mathbf{u}_w = (\pm 0.2, 0)$.

L^2 errors of the velocity field \mathbf{u} , pressure p , and phase variable ϕ are calculated at time $T = 1$, with a reference solution obtained using the finest resolution of $n_x = 511, n_y = 64$. Similarly, in Fig. 4 (b), to test the convergence in y -direction, we fix the number of Fourier modes $n_x = 511$ for a series of n_y starting from 8 with an increment 8. The L^2 errors of the velocity field \mathbf{u} , pressure p , and phase variable ϕ are again calculated at $T = 1$ with the reference solution using the finest resolutions of $n_x = 511$ and $n_y = 64$. We see that the proposed numerical schemes can achieve spectral accuracy in L^2 norm for both velocity and phase variable. The convergence of pressure in y direction doesn't have spectral order because an artificial implicit boundary condition $\partial p / \partial n = 0$ is used for pressure in equation (3.76).

To test the convergence for temporal discretization, we fix the spatial resolution as $n_x = 511, n_y = 64$ so that the errors from the spatial discretization are negligible compared to the temporal discretization errors, and perform the refinement test of the time step for the schemes CN2 and BDF2. We choose the approximate solution using the scheme BDF2 with the time step size $\delta t = 2.5 \times 10^{-4}$ as the benchmark solution (approximately the exact solution) for computing errors. In Fig. 5, we present the L^2 errors of the velocity field \mathbf{u} and the phase field variable ϕ between the numerical solution and the exact solution at $T = 0.4$ with different time step sizes $\delta t = 0.016/2^k, k = 0, 1, \dots, 5$. The results obtained by CN2 and BDF2 schemes are shown together with the results obtained by the first order linear stabilization scheme (denoted by LSS) proposed in [56] for comparisons. We observe that both CN2 and BDF2 schemes are second order accurate for the velocity field \mathbf{u} as well as the phase field variable ϕ , which provide much more accurate results than that of the first order LSS scheme.

5.1.2. Energy dissipation and volume preservation. For both CN2 and BDF2 schemes, we test the energy dissipation for the isolated system by setting the wall velocity $\mathbf{u}_w = 0$, and further compare the evolution of the free energy functional for four different time step sizes where $\delta t = 0.01, 0.005, 0.002$ and 0.0001 for the default parameters (5.1) until $T = 2.5$ in Fig. 6. For either scheme, we observe that all energy curves show the decays, that confirm that our algorithms are unconditionally stable for any time step size. For smaller time steps of $\delta t = 0.0001, 0.005, 0.002$,

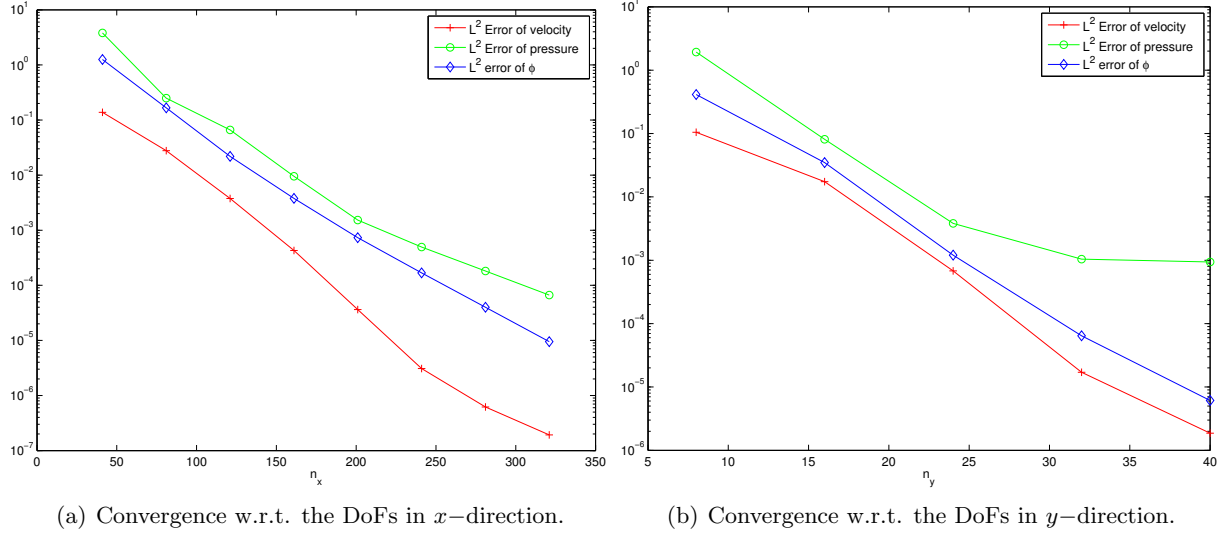


FIG. 4. The spatial convergence tests for L^2 error of the velocity, the pressure and the phase field variable at $T = 1$ using the BDF2 scheme with the time step $\delta t = 0.0005$. (a): the L^2 error with respect to number of DoFs in x -direction; (b): the convergence with respect the number of DoFs in y -direction.

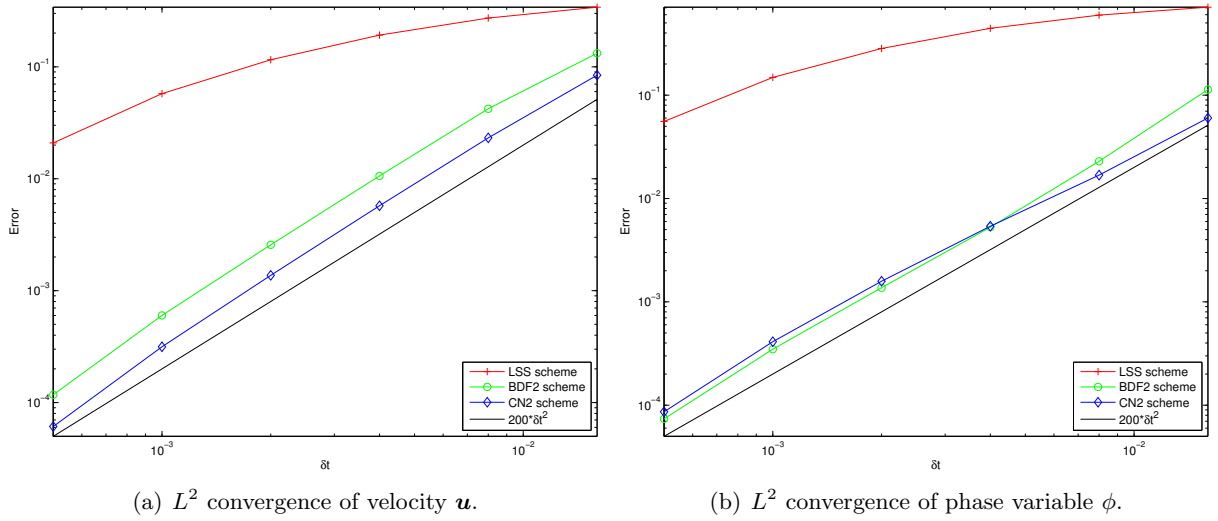


FIG. 5. The temporal mesh refinement tests for the velocity field \mathbf{u} (a) and the phase field variable ϕ (b) obtained by CN2 scheme, BDF2 scheme, and the first order scheme (denoted by LSS) proposed in [56]. The axes are in loglog scales, a line with slope 2 in black color is plotted to show the second order convergence of the CN2 and BDF2 schemes.

the three energy curves coincide very well. But for the larger time step of $\delta t = 0.01$, the energy

curve is considerable (but not very far) away from others. This means the time step size has to be smaller than 0.01 at least, in order to get reasonably good accuracy.

In Fig.7, we show the time evolution for the volume difference $V(t) - V_0$ where $V(t) = \int_{\Omega} \phi(x, t) d\mathbf{x}$ and $V_0 = \int_{\Omega} \phi_0(x) d\mathbf{x}$ for the numerical solutions obtained by the schemes CN2 and BDF2, we observe that the volume difference is very close to the machine precision.

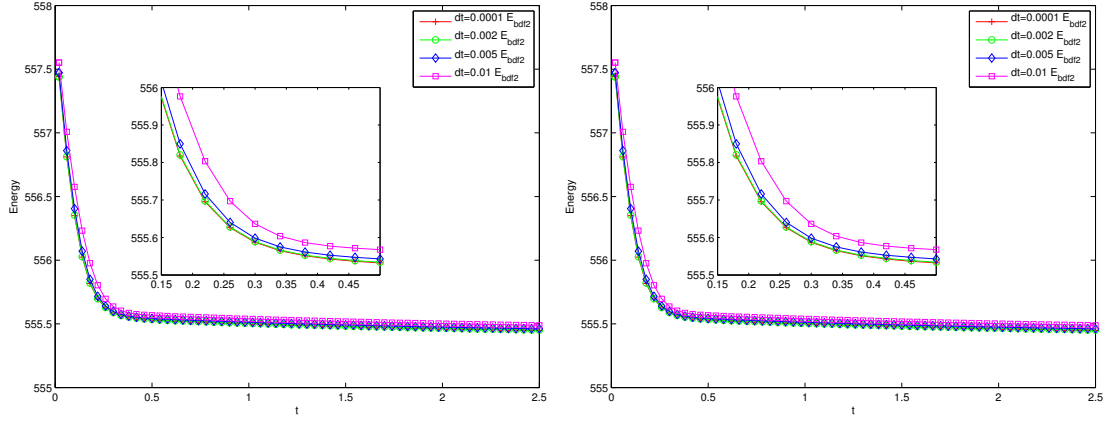


FIG. 6. The discrete energy dissipation of CN2 (left) and BDF2 (right) schemes for several time steps. $u_w = 0$ and other parameters are given in (5.1).

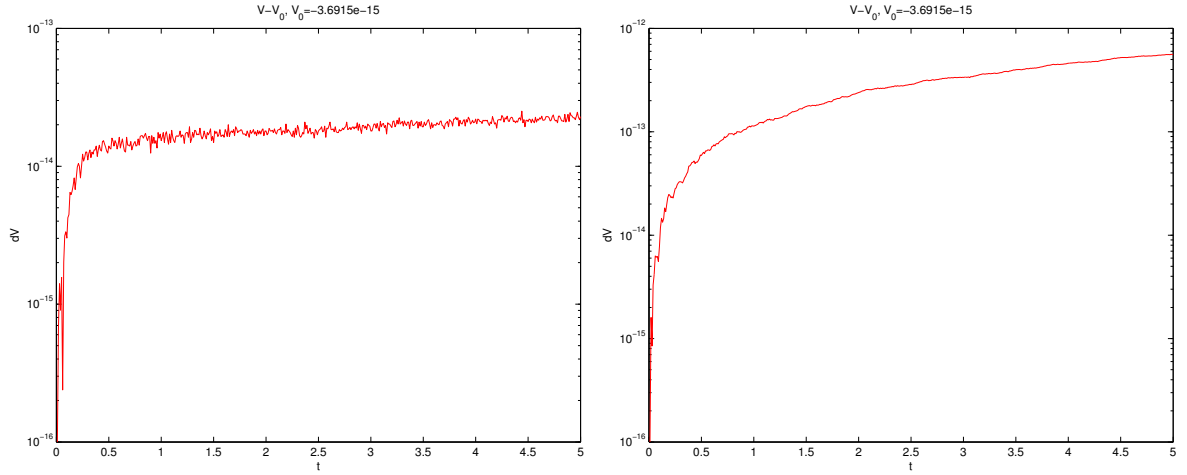


FIG. 7. Volume conservation property of CN2 (left) and BDF2 (right) schemes.

5.1.3. Efficiency. In Table 1 and Table 2, we show the number of iterations needed by the BiCGSTAB solver for the CN2 and BDF2 schemes. The default parameters are $n_x = 257, n_y = 32, \delta t = 0.01, \gamma = 500, \lambda = 12$. We vary these parameters one by one while fixing the rest of them to be default values. In Table 1, the number of iterations are always around $O(10)$ for various grid points and γ , that means the number of iterations actually does not show any dependence on the number of spatial grid points and the parameter γ . In Table 2, when we vary the time step δt and parameter

λ , we can see that larger values of them can cause significant increase for the number of iterations. Namely, when δt and λ are larger, the conditional numbers of the linear system become worse that is reasonable and can be easily observed from the format of the linear system (3.38).

$n_x \times n_y$	129×16	257×32	513×64	γ	100	10	1
CN2	8	8.7	9.6	CN2	7.9	9	9
BDF2	8.5	8.5	8.5	BDF2	9.1	10.0	10.1

TABLE 1. The average number of the inner iterations for BiCGSTAB with respect to the grid points $n_x \times n_y$ and the parameter γ . The tolerance is 10^{-8} for schemes CN2 and BDF2. The default values are $n_x = 257, n_y = 32, \delta t = 0.01, \gamma = 500, \lambda = 12$.

δt	0.001	0.1	1	λ	1	60	144
CN2	3.8	27	68	CN2	5	19.6	35.5
BDF2	4	27	69.6	BDF2	5	20.8	42.5

TABLE 2. The average number of the inner iterations for BiCGSTAB with respect to the time step δt and the parameter λ . The tolerance is 10^{-8} for both schemes CN2 and BDF2. The default values are $n_x = 257, n_y = 32, \delta t = 0.01, \gamma = 500, \lambda = 12$.

5.2. A drop under shear flow. In this example, we simulate the dynamics of a shear drop using the scheme BDF2. The computed domain is $[0, L_x] \times [-1, 1]$ with $L_x = 10$. The wall velocity $\mathbf{u}_w = (\pm 2, 0)$ and all other parameters are given in (5.1).

Fig.8 illustrates the dynamical motions of a drop under shear with an acute contact angle $\theta_s = \pi/6$ until $T = 5$. Initially, the drop is set in the middle of the bottom plate, as shown in the first subfigure. As the bottom plate moves, the drop also moves with the plate but at a much smaller velocity. This means the drop slips on the bottom plate. As time goes on, the contact region of the drop with the bottom boundary gets smaller and smaller. It eventually gets off the bottom boundary around $t = 3$ and moves toward the center of the channel. We also simulate an obtuse contact angle $\theta_s = 2\pi/3$ case, in which the drop is harder to get off the bottom boundary, which is shown in Fig.9.

5.3. A dripping drop. As the last example, we simulate the dynamics of a dripping drop driven by the gravity force. We consider the case where the density difference of the drop and ambient fluid is small so that we can use the Boussinesq approximation [32, 67] in the momentum equation as follows:

$$(5.3) \quad \rho_0(\mathbf{u}_t + (\mathbf{u} \cdot \nabla)\mathbf{u}) + \nabla p - \nu \nabla^2 \mathbf{u} + \phi \nabla \mu = f_{\mathbf{a}},$$

where $f_{\mathbf{a}} = -((1 + \phi)(\rho_1 - \rho_0) + (1 - \phi)(\rho_2 - \rho_0))\mathbf{a}_0$, $\mathbf{a}_0 = (0, a_0)$ is the gravity acceleration. We set $\rho_1 = 2, \rho_2 = 1, \rho_0 = (\rho_1 + \rho_2)/2 = 1.5$ and $a_0 = 20$. The computed domain is $[0, 1.6] \times [-1, 1]$.

Fig.10 illustrates the dynamics of a drop with an obtuse static contact angle $\theta_s = 2\pi/3$. The drop (half circle with contact angle $\pi/2$) is set in the middle of the top plate initially, and reshapes

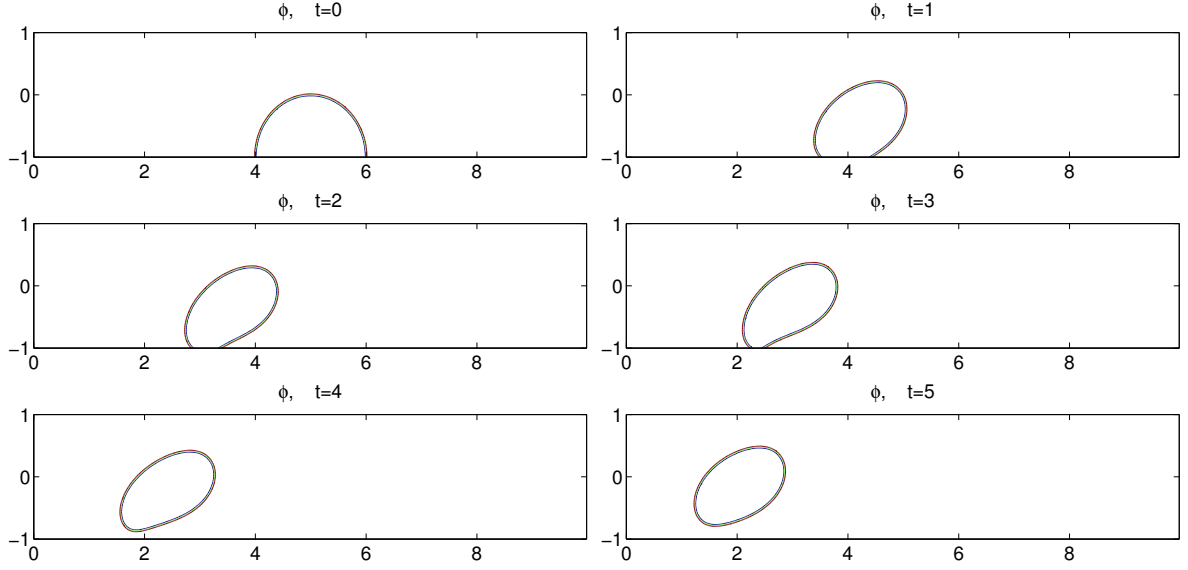


FIG. 8. The dynamical behaviors of a drop in shear flow simulated using the BDF2 scheme. Snapshots are taken at $t = 0, 1, 2, 3, 4, 5$. We take the wall velocity $\mathbf{u}_w = (\pm 2, 0)$ and the static contact angle $\theta_s = \pi/6$.

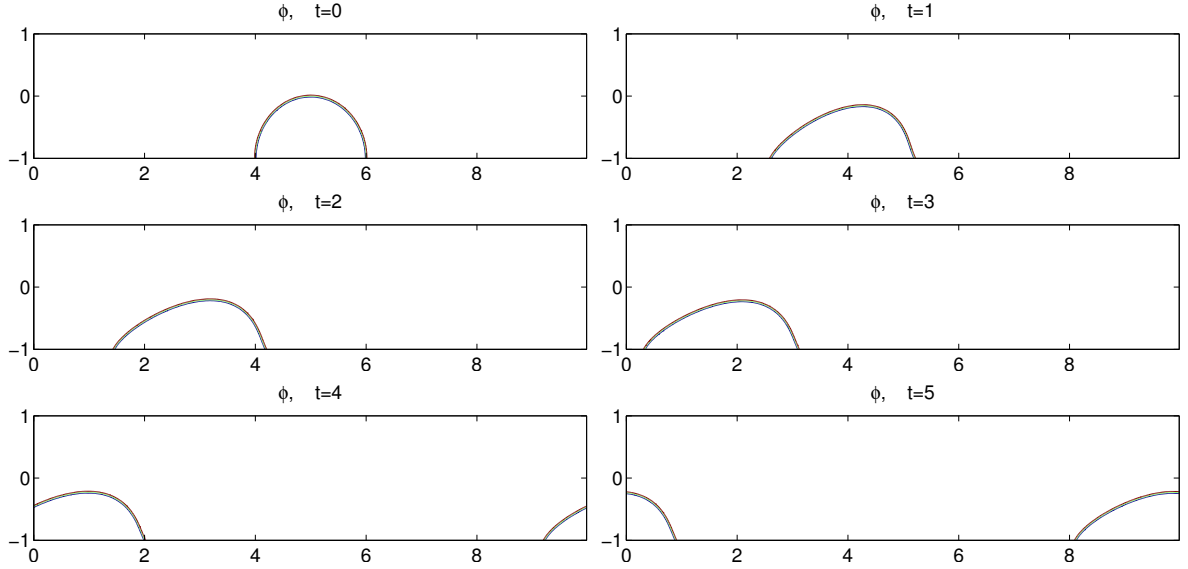


FIG. 9. The dynamical behaviors of a drop in shear flow using the BDF2 scheme. Snapshots are taken at $t = 0, 1, 2, 3, 4, 5$. We take the wall velocity $\mathbf{u}_w = (\pm 2, 0)$ and the static contact angle $\theta_s = 2\pi/3$.

its contact angle from $\pi/2$ to θ_s . The equilibrium solution that the drop is still adhered to the top wall is obtained at $t = 5$.

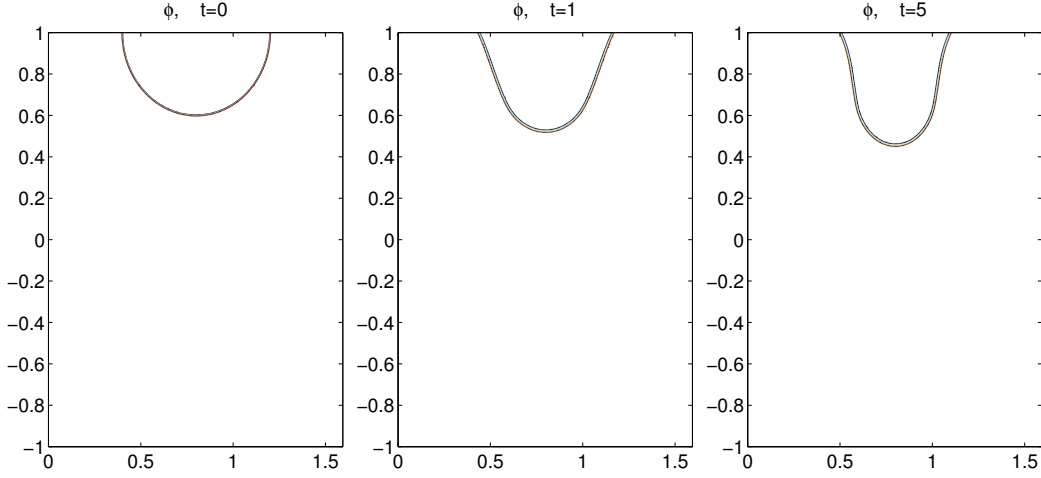


FIG. 10. A drop with obtuse contact angle in gravitational flow. Results are obtained using BDF2 scheme. $\mathbf{u}_w = 0$, $\theta_s = 2\pi/3$, $a_0 = 20$.

In Fig. 11, we set the static contact angle $\theta_s = \pi/4$ and keep all equation parameters same as the previous example. As the obtuse contact angle case, at the initial stage of dripping, the drop reshapes its contact angle from $\pi/2$ to θ_s , see $t = 1$. Then it slowly drips off from the top plate due to the buoyancy force, and finally touches to the bottom plate and stay there with a contact angle very close to $\pi/4$.

From the simulations shown Fig. 10 and Fig. 11, we know that drops with the obtuse static contact angle is relatively harder to drip off from the plate in comparison with the acute contact angle. Therefore, to see the dripping drip with the obtuse static contact angle, we need increase the gravitational force. Finally, we set the contact angle $\theta_s = 2\pi/3$ as Fig. 10 but improving the gravity force to be $a_0 = 33$, we observe that the drop drips off from the top plate as well, however, there is still a part of the drop adhered to the top plate, see the snapshots at $t = 3, 4, 5$ in Fig. 12.

6. CONCLUDING REMARKS

Although the Cahn-Hilliard phase field model with moving contact line boundary conditions had been well studied for more than a decade, the development of efficient energy stable schemes with second order accuracy still remained very scarce due to its complex nature of nonlinearities in the bulk and on the boundary. In this paper, by combining the projection method for Navier-Stokes equations, the newly developed IEQ method for the nonlinear bulk and boundary energy potential, and a subtle explicit-implicit technique for the stress and convective terms, we construct two linear, second order temporal discretization schemes for solving this model. The well-posedness of the linear systems and their energy stabilities are proved rigorously. While we have considered only time discretizations here, the results can carry over to any consistent finite-dimensional Galerkin (finite element or spectral) approximations since the proofs are all based on variational formulations with all test functions in the same space as the trial function. We also performed a number of numerical results to validate the accuracy, stability and efficiency of the proposed schemes.

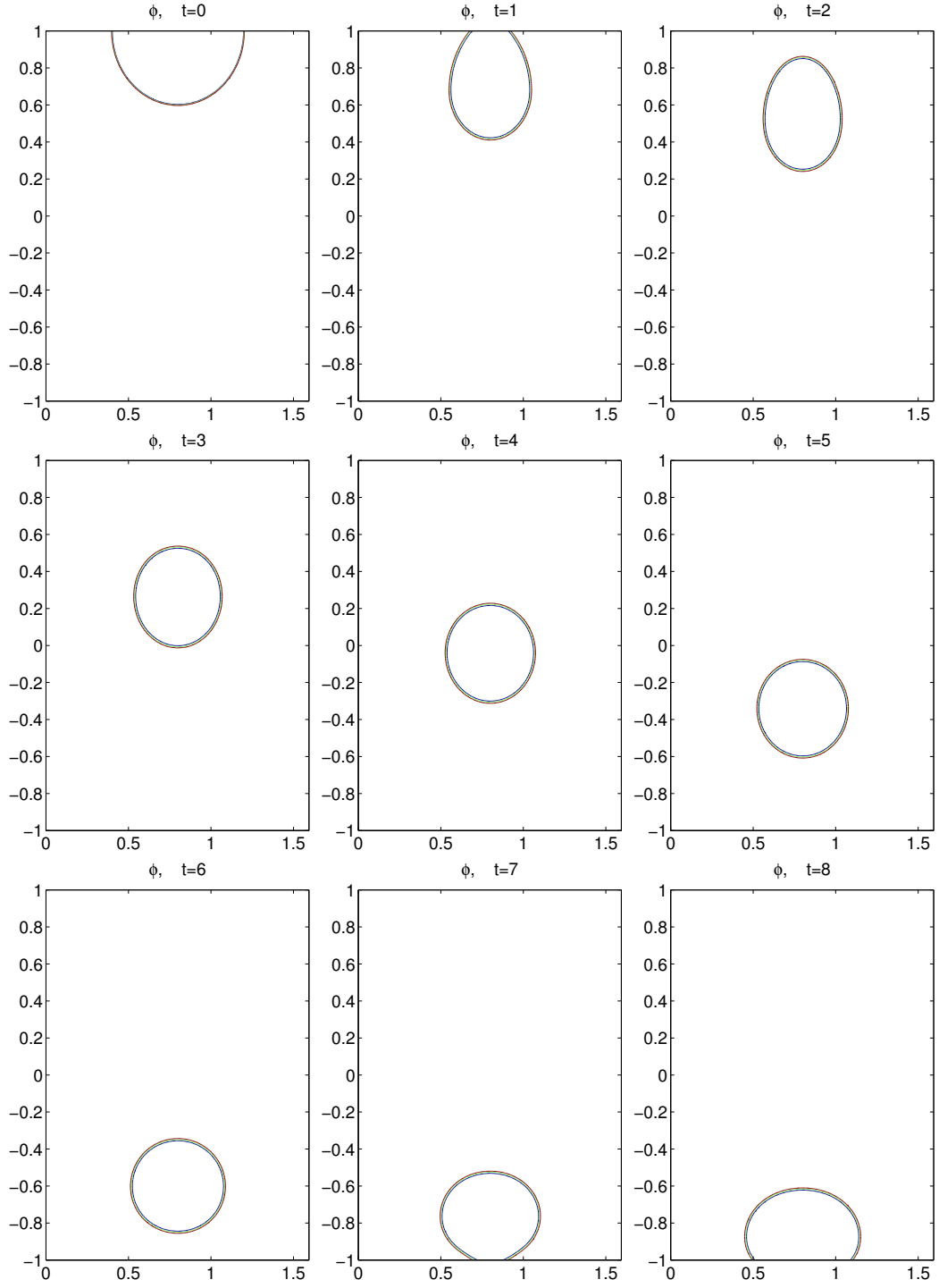


FIG. 11. A drop with acute static contact angle drips in gravitational flow. Results are obtained using BDF2 scheme. $\mathbf{u}_w = 0$, $\theta_s = \pi/4$, $a_0 = 20$.

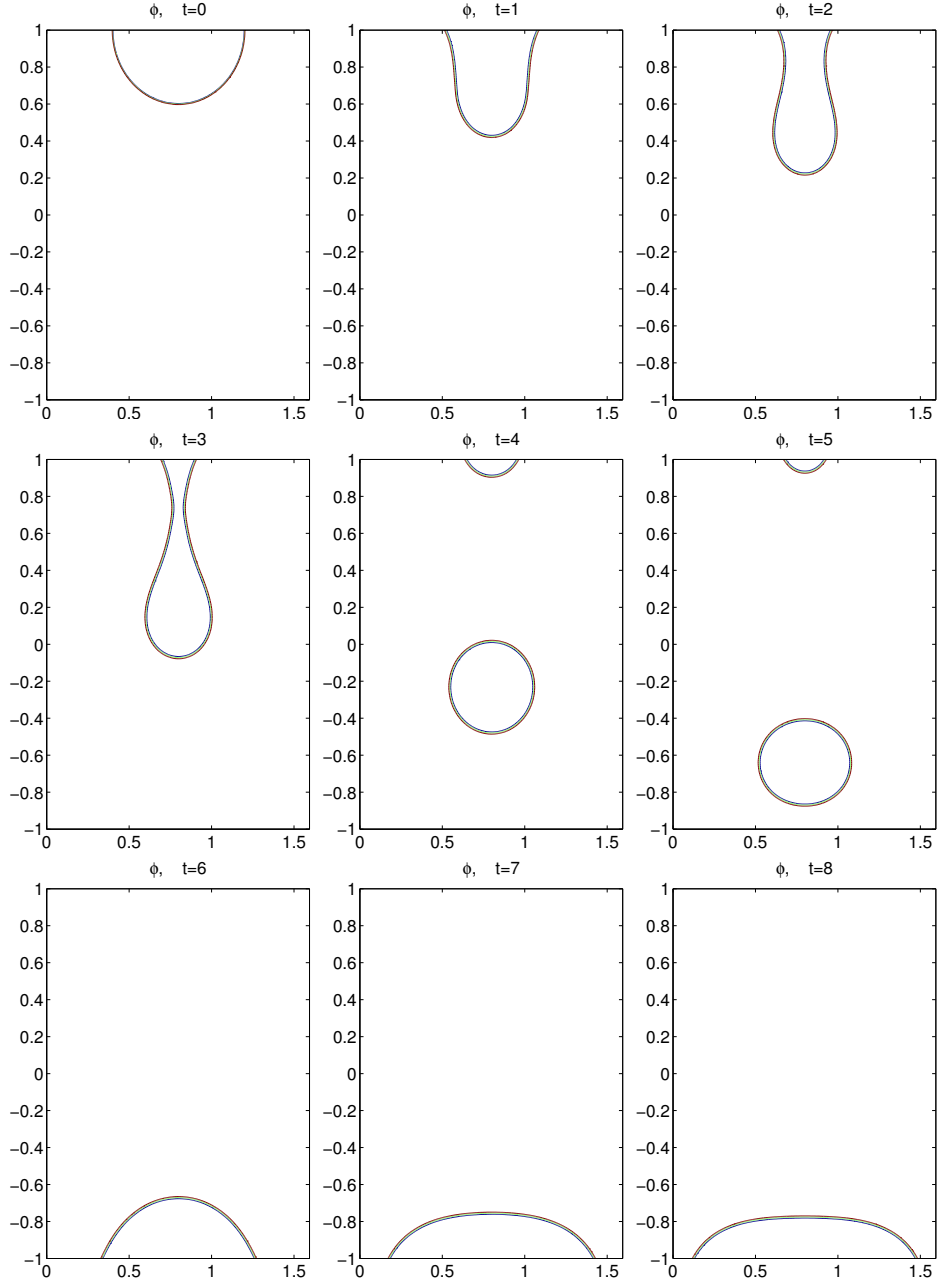


FIG. 12. A drop with obtuse contact angle drips in gravitational flow. Results are obtained using BDF2 scheme. $\mathbf{u}_w = 0$, $\theta_s = 2\pi/3$, $a_0 = 33$.

ACKNOWLEDGMENTS

The work of X. Yang is partially supported by the National Science Foundation under grant number DMS-1200487 and NSF DMS-1418898. The work of H. Yu is partially supported by China National Program on Key Basic Research Project 2015CB856003 and NSFC 91530322, 11371358.

REFERENCES

- [1] S. Aland and F. Chen. An efficient and energy stable scheme for a phase-field model for the moving contact line problem. *Int. J. Num. Meth. Fluids.*, 81:657–671, 2015.
- [2] F. Boyer and C. Lapuerta. Study of a three component Cahn–Hilliard flow model. *ESAIM: Math. Modelling. Num. Ana.*, 40(4):653–687, 2006.
- [3] F. Boyer, C. Lapuerta, S. Minjeaud, B. Piar, and M. Quintard. Cahn–Hilliard/navier-stokes model for the simulation of three-phase flows. *Transp Porous Med.*, 82:463–483, 2010.
- [4] F. Boyer and S. Minjeaud. Numerical schemes for a three component Cahn–Hilliard model. *ESAIM: Mathematical Modelling and Numerical Analysis*, 45(04):697–738, 2011.
- [5] J. W. Cahn and J. E. Hilliard. Free energy of a nonuniform system. I. interfacial free energy. *J. Chem. Phys.*, 28:258–267, 1958.
- [6] R. Chen, G. Ji, X. Yang, and H. Zhang. Decoupled energy stable schemes for phase-field vesicle membrane model. *J. Comput. Phys.*, 302:509–523, 2015.
- [7] S. Dong. On imposing dynamic contact-angle boundary conditions for wall-bounded liquid-gas flows. *Comput. Meth. Appl. Mech. and Engrg.*, 247-248:179–200, 2012.
- [8] S. Dong and J. Shen. A time-stepping scheme involving constant coefficient matrices for phase-field simulations of two-phase incompressible flows with large density ratios. *J. Comput. Phys.*, 231(17):5788–5804, 2012.
- [9] E. B. Dussan. On the spreading of liquids on solid surfaces: Static and dynamic contact lines. *Annual Review of Fluid Mechanics*, 11(1):371–400, 1979.
- [10] E. B. Dussan and S. H. Davis. On the motion of a fluid-fluid interface along a solid surface. *J. Fluid. Mech.*, 65(01):71–95, 1974.
- [11] W. E and J-G. Liu. Projection method. I. Convergence and numerical boundary layers. *SIAM J. Numer. Anal.*, 32(4):1017–1057, 1995.
- [12] D. J. Eyre. Unconditionally gradient stable time marching the Cahn–Hilliard equation. In *Computational and mathematical models of microstructural evolution (San Francisco, CA, 1998)*, volume 529 of *Mater. Res. Soc. Sympos. Proc.*, pages 39–46. MRS, 1998.
- [13] J. J. Feng, C. Liu, J. Shen, and P. Yue. An energetic variational formulation with phase field methods for interfacial dynamics of complex fluids: advantages and challenges. *IMA volumes in Mathematics and Applications*, 140:1–26, 2005.
- [14] X. Feng and A. Prohl. Numerical analysis of the Allen–Cahn equation and approximation for mean curvature flows. *Numer. Math.*, 94:33–65, 2003.
- [15] X. Feng and A. Prohl. Analysis of a fully discrete finite element method for the phase field model and approximation of its sharp interface limits. *Math. Comp.*, 73:541–567, 2004.
- [16] M. Gao and X-P. Wang. A gradient stable scheme for a phase field model for the moving contact line problem. *J. Comput. Phys.*, 231(4):1372–1386, 2012.
- [17] M. Gao and X-P. Wang. An efficient scheme for a phase field model for the moving contact line problem with variable density and viscosity. *J. Comput. Phys.*, 272:704–718, 2014.
- [18] J. L. Guermond, P. Mineev, and J. Shen. An overview of projection methods for incompressible flows. *Comput. Methods Appl. Mech. Engrg.*, 195:6011–6045, 2006.
- [19] F. Guillén-González and G. Tierra. On linear schemes for a Cahn–Hilliard diffuse interface model. *J. Comput. Phys.*, 234:140–171, 2013.
- [20] Z. Guo, P. Lin, and J. S. Lowengrub. A numerical method for the quasi-incompressible Cahn–Hilliard–Navier–Stokes equations for variable density flows with a discrete energy law. *Journal of Computational Physics*, 276:486–507, 2014.
- [21] D. Han, A. Brylev, X. Yang, and Z. Tan. Numerical analysis of second order, fully discrete energy stable schemes for phase field models of two phase incompressible flows. *J. Sci. Comput.*, 70:965–989, 2017.
- [22] D. Han and X. Wang. A second order in time, uniquely solvable, unconditionally stable numerical scheme for Cahn–Hilliard–Navier–Stokes equation. *J. Comput. Phys.*, 290:139–156, 2015.
- [23] Q. He, R. Glowinski, and X-P. Wang. A least-squares/finite element method for the numerical solution of the Navier–Stokes–Cahn–Hilliard system modeling the motion of the contact line. *J. Comput. Phys.*, 230(12):4991–5009, 2011.
- [24] J. Hua, P. Lin, C. Liu, and Q. Wang. Energy law preserving c0 finite element schemes for phase field models in two-phase flow computations. *J. Comput. Phys.*, 230:7155–7131, 2011.
- [25] R. Ingram. A new linearly extrapolated Crank–Nicolson time-stepping scheme for the Navier–Stokes equations. *Math. Comp.*, 82(284):1953–1973, 2013.

- [26] D. Jacqmin. Contact-line dynamics of a diffuse fluid interface. *Journal of Fluid Mechanics*, 402:57–88, 2000.
- [27] J. Kim. Phase field computations for ternary fluid flows. *Comput. Meth. Appl. Mech. Engrg.*, 196:4779–4788, 2007.
- [28] J. Kim and J. Lowengrub. Phase field modeling and simulation of three-phase flows. *Interfaces and Free Boundaries*, 7:435–466, 2005.
- [29] J. Koplik, J. R. Banavar, and J. F. Willemsen. Molecular dynamics of Poiseuille flow and moving contact lines. *Phys. Rev. Lett.*, 60(13):1282–1285, 1988.
- [30] J. Koplik, J. R. Banavar, and J. F. Willemsen. Molecular dynamics of fluid flow at solid surfaces. *Phys. Fluids A*, 1:781–794, 1989.
- [31] J. Li and Q. Wang. Mass conservation and energy dissipation issue in a class of phase field models for multiphase fluids. *J. of Appl. Mech.*, 81(2):021004, 2013.
- [32] C. Liu and J. Shen. A phase field model for the mixture of two incompressible fluids and its approximation by a Fourier-spectral method. *Physica D*, 179(3-4):211–228, 2003.
- [33] C. Liu, J. Shen, and X. Yang. Dynamics of defect motion in nematic liquid crystal flow: Modeling and numerical simulation. *Comm. in Comput. Phys.*, 2:1184–1198, 2007.
- [34] C. Liu, J. Shen, and X. Yang. Decoupled energy stable schemes for a phase-field model of two-phase incompressible flows with variable density. *J. Sci. Comput.*, 62:601–622, 2015.
- [35] J. Lowengrub and L. Truskinovsky. Quasi-incompressible Cahn-Hilliard fluids and topological transitions. *R. Soc. Lond. Proc. Ser. A Math. Phys. Eng. Sci.*, 454(1978):2617–2654, 1998.
- [36] L. Ma, R. Chen, X. Yang, and H. Zhang. Numerical approximations for Allen-Cahn type phase field model of two-phase incompressible fluids with moving contact lines. *Comm. Comput. Phys.*, 21:867–889, 2017.
- [37] C. Miehe, M. Hofacker, and F. Welschinger. A phase field model for rate-independent crack propagation: Robust algorithmic implementation based on operator splits. *Comput. Meth. in Appl. Mech. Engrg.*, 199:2765–2778, 2010.
- [38] S. Minjeaud. An unconditionally stable uncoupled scheme for a triphasic Cahn-Hilliard/Navier-Stokes model. *Numerical Methods for Partial Differential Equations*, 29:584–618, 2013.
- [39] N. Moelans, B. Blanpain, and P. Wollants. A phase field model for grain growth and thermal grooving in thin films with orientation dependent surface energy. *Solid State Phenomena*, 129:89–94, 2007.
- [40] H. K. Moffatt. Viscous and resistive eddies near a sharp corner. *J. Fluid Mech.*, 18(01):1–18, 1964.
- [41] R. H. Nochetto, A. J. Salgado, and I. Tomas. A diffuse interface model for two-phase ferrofluid flows. *Comput. Meth. in Appl. Mech. and Engrg.*, 309:497–531, 2016.
- [42] T. Qian, X-P. Wang, and P. Sheng. Molecular scale contact line hydrodynamics of immiscible flows. *Phys. Rev. E.*, 68(1):016306, 2003.
- [43] T. Qian, X-P. Wang, and P. Sheng. Power-law slip profile of the moving contact line in two-phase immiscible flows. *Phys. Rev. Lett.*, 93:094501, 2004.
- [44] T. Qian, X-P. Wang, and P. Sheng. A variational approach to moving contact line hydrodynamics. *J. Fluid Mech.*, 564:333–360, 2006.
- [45] A. J. Salgado. A diffuse interface fractional time-stepping technique for incompressible two-phase flows with moving contact lines. *ESAIM: M2NA*, 47:743–769, 2013.
- [46] J. Shen. On error estimates of the projection methods for the Navier-Stokes equations: second-order schemes. *Math. Comp.*, 65(215):1039–1065, 1996.
- [47] J. Shen, T. Tang, and J. Yang. On the maximum principle preserving schemes for the generalized Allen-Cahn equation. *Comm. Math. Sci.*, 14:1517–1534, 2016.
- [48] J. Shen, C. Wang, S. Wang, and X. Wang. Second-order convex splitting schemes for gradient flows with ehrlich-schwoebel type energy: application to thin film epitaxy. *SIAM. J. Numer. Anal.*, 50:105–125, 2012.
- [49] J. Shen and X. Yang. An efficient moving mesh spectral method for the phase-field model of two-phase flows. *J. Comput. Phys.*, 228:2978–2992, 2009.
- [50] J. Shen and X. Yang. Energy stable schemes for Cahn-Hilliard phase-field model of two-phase incompressible flows. *Chinese Ann. Math. series B*, 31:743–758, 2010.
- [51] J. Shen and X. Yang. Numerical approximations of Allen-Cahn and Cahn-Hilliard equations. *Disc. Cont. Dyn. Sys. A*, 28:1669–1691, 2010.
- [52] J. Shen and X. Yang. A phase-field model and its numerical approximation for two-phase incompressible flows with different densities and viscosities. *SIAM J. Sci. Comput.*, 32:1159–1179, 2010.
- [53] J. Shen and X. Yang. Decoupled energy stable schemes for phase field models of two phase complex fluids. *SIAM J. Sci. Comput.*, 36:B122–B145, 2014.

- [54] J. Shen and X. Yang. Decoupled, energy stable schemes for phase-field models of two-phase incompressible flows. *SIAM J. Num. Anal.*, 53(1):279–296, 2015.
- [55] J. Shen, X. Yang, and Q. Wang. On mass conservation in phase field models for binary fluids. *Comm. Comput. Phys.*, 13:1045–1065, 2012.
- [56] J. Shen, X. Yang, and H. Yu. Efficient energy stable numerical schemes for a phase field moving contact line model. *J. Comput. Phys.*, 284:617–630, 2015.
- [57] J. Shin, Y. Choi, and J. Kim. An unconditionally stable numerical method for the viscous Cahn–Hilliard equation. *Disc. Cont. Dyn. Sys. B*, 19:1734–1747, 2014.
- [58] R. Spatschek, E. Brener, and A. Karma. A phase field model for rate-independent crack propagation: Robust algorithmic implementation based on operator splits. *Philos. Mag.*, 91:75–95, 2010.
- [59] R. Spatschek, M. Hartmann, E. Brener, H. Muller-Krumbhaar, and K. Kassner. Phase field modeling of fast crack propagation. *Phys. Rev. Lett.*, 96:015502, 2006.
- [60] P. Sun, C. Liu, and J. Xu. Phase field model of thermo-induced marangoni effects in the mixtures and its numerical simulations with mixed finite element methods. *Comm. in Comput. Phys.*, 6:1095–1117, 2009.
- [61] P. A. Thompson and M. O. Robbins. Simulations of contact-line motion: Slip and the dynamic contact angle. *Phys. Rev. Lett.*, 63(7):766–769, 1989.
- [62] J. van Kan. A second-order accurate pressure-correction scheme for viscous incompressible flow. *SIAM J. Sci. Statist. Comput.*, 7(3):870–891, 1986.
- [63] L. Vanherpe, N. Moelans, B. Blanpain, and S. Vandewalle. Bounding box framework for efficient phase field simulation of grain growth in anisotropic systems. *Comput. Materials Sci.*, 50:2221–2231, 2011.
- [64] C. Wang and S. M. Wise. An energy stable and convergent finite-difference scheme for the modified phase field crystal equation. *SIAM J. Numer. Anal.*, 49:945–969, 2011.
- [65] C. Xu and T. Tang. Stability analysis of large time-stepping methods for epitaxial growth models. *SIAM J. Num. Anal.*, 44:1759–1779, 2006.
- [66] X. Yang. Linear, first and second order and unconditionally energy stable numerical schemes for the phase field model of homopolymer blends. *J. Comput. Phys.*, 327:294–316, 2016.
- [67] X. Yang, J. J. Feng, C. Liu, and J. Shen. Numerical simulations of jet pinching-off and drop formation using an energetic variational phase-field method. *J. Comput. Phys.*, 218:417–428, 2006.
- [68] X. Yang, M. G. Forest, H. Li, C. Liu, J. Shen, Q. Wang, and F. Chen. Modeling and simulations of drop pinch-off from liquid crystal filaments and the leaky liquid crystal faucet immersed in viscous fluids. *J. Comput. Phys.*, 236:1–14, 2013.
- [69] X. Yang and D. Han. Linearly first- and second-order, unconditionally energy stable schemes for the phase field crystal equation. *J. Comput. Phys.*, 330:1116–1134, 2017.
- [70] X. Yang and L. Ju. Efficient linear schemes with unconditionally energy stability for the phase field elastic bending energy model. *Comput. Meth. Appl. Mech. Engrg.*, 315:691–712, 2017.
- [71] X. Yang and J. Lu. Linear and unconditionally energy stable schemes for the binary fluid-surfactant phase field model. *in press*, DOI: 10.1016/j.cma.2017.02.011, *Comput. Meth. Appl. Mech. Engrg.*, 2017.
- [72] X. Yang, J. Zhao, and Q. Wang. Numerical approximations for the molecular beam epitaxial growth model based on the invariant energy quadratization method. *J. Comput. Phys.*, 333:104–127, 2017.
- [73] X. Yang, J. Zhao, Q. Wang, and J. Shen. Numerical approximations for a three components Cahn–Hilliard phase-field model based on the invariant energy quadratization method. *arXiv:1701.07469*, 2017.
- [74] H. Yu and X. Yang. Decoupled energy stable schemes for phase field model with contact lines and variable densities. *J. Comput. Phys.*, 334:665–686, 2017.
- [75] P. Yue, C. Zhou, and J. J. Feng. Sharp-interface limit of the Cahn–Hilliard model for moving contact lines. *J. Fluid Mech.*, 645:279–294, 2010.
- [76] J. Zhao, H. Li, Q. Wang, and X. Yang. A linearly decoupled energy stable scheme for phase-field models of three-phase incompressible flows. *J. Sci. Comput.*, 70:1367–1389, 2017.
- [77] J. Zhao, Q. Wang, and X. Yang. Numerical approximations to a new phase field model for immiscible mixtures of nematic liquid crystals and viscous fluids. *Comput. Meth. Appl. Mech. Engrg.*, 310:77–97, 2016.
- [78] J. Zhao, X. Yang, J. Li, and Q. Wang. Energy stable numerical schemes for a hydrodynamic model of nematic liquid crystals. *SIAM. J. Sci. Comput.*, 38:A3264–A3290, 2016.
- [79] J. Zhao, X. Yang, J. Shen, and Q. Wang. A decoupled energy stable scheme for a hydrodynamic phase-field model of mixtures of nematic liquid crystals and viscous fluids. *J. Comput. Phys.*, 305:539–556, 2016.